The Urban Heat Island of Wageningen

High spatial resolution measurements and temperature projections into the future

Michiel van der Harst

The urban heat island of Wageningen

High spatial resolution measurements and temperature projections into the future

Michiel van der Harst

Student Climate Studies

891020307060

Meteorology and Air Quality

MAQ-80836

2014-04-13

Supervisors:

Bert Heusinkveld

Reinder Ronda

Gert-Jan Steeneveld

Contents

1. Introduction

More than 50 % of world population is living in cities at this moment and this will increase to 60 % in 2030 and 67 % in 2050 (UN, 2011). These urban areas experience different meteorological conditions than their rural surroundings (Arnfield, 2003, Oke, 1982). The physical properties of cities and buildings results in a modification of surface radiation and the energy budget (Taha, 1997, Doll et al., 1985, XIAO et al., 2007, Harman et al., 2004, Tsangrassoulis and Santamouris, 2003). Daytime heat storage in buildings and the subsequent heat release after sunset results in a nocturnal urban heat island: a higher temperature in urban areas than in their rural counterparts (Arnfield, 2003, Oke, 1982) and a variation of temperature within the city (Spronken-Smith and Oke, 1999, Stewart and Oke, 2012, Stewart, 2011). The urban heat island combined with climate change can results in enhancement of harmful conditions for the urban populations (Parry, 2007).

Urban heat islands (UHI) in the Netherlands have been documented only superficially. Because the Netherlands is located in a mild (Cfb type) climate, close to sea (Peel et al., 2007), the UHI was hypothesized to be relatively small and unimportant. However, substantial urban heat islands of 7 and 8 °C, have been found in Utrecht in the 1970s (Floor, 1970, Conrads, 1975) and in Rotterdam in the 1980s (Roodenburg, 1983), respectively. Despite the significant UHIs found in Utrecht and Rotterdam, no more research was conducted in the Netherlands until 2010, when a maximum UHI[1] of 8 K for Rotterdam and 7 K for Arnhem was found (Heusinkveld et al., 2012, Heusinkveld et al., 2010). Steeneveld et al. (2011) reports an average daily maximum UHI of 2.3 K in 23 Dutch cities of variable size and urban morphology, based on hobby meteorological stations.

The urban heat island is caused by the modification of the radiation and energy budget with respect to rural situation.

The radiation budget consist of the sum of incoming and outgoing shortwave radiation ($K\downarrow$ and $K\uparrow$, respectively) and incoming and outgoing longwave radiation ($L\downarrow$ and $L\uparrow$ respectively) that are equal to the flux density of net all-wave radiation (Q*) (Eq. 1), in which transporting energy to the surface is considered positive and transporting energy away from the surface is negative. In other words: the available energy is determined by the received and emitted radiation.

Eq. 1 $$Q^* = K\downarrow + K\uparrow + L\downarrow + L\uparrow$$

If urban and rural surroundings are compared it is noticed that all radiation terms are altered. Incoming shortwave radiation ($K\downarrow$) is influenced by object, but is of similar size as in rural surroundings (Christen and Vogt, 2004). The outgoing shortwave radiation is higher in urban areas due to lower albedo (Christen and Vogt, 2004), resulting in higher net shortwave radiation input in the urban areas. This is mostly offset by larger loss through longwave radiation (Christen and Vogt, 2004). The daily circle of energy is enhanced in urban surroundings, resulting in a higher net all-wave radiation flux during the day and lower during night-time (Figure 1.c).

[1] The 7 and 8 K UHI found by Heusinkveld was the maximum difference between the urban and rural temperature over a long time series.

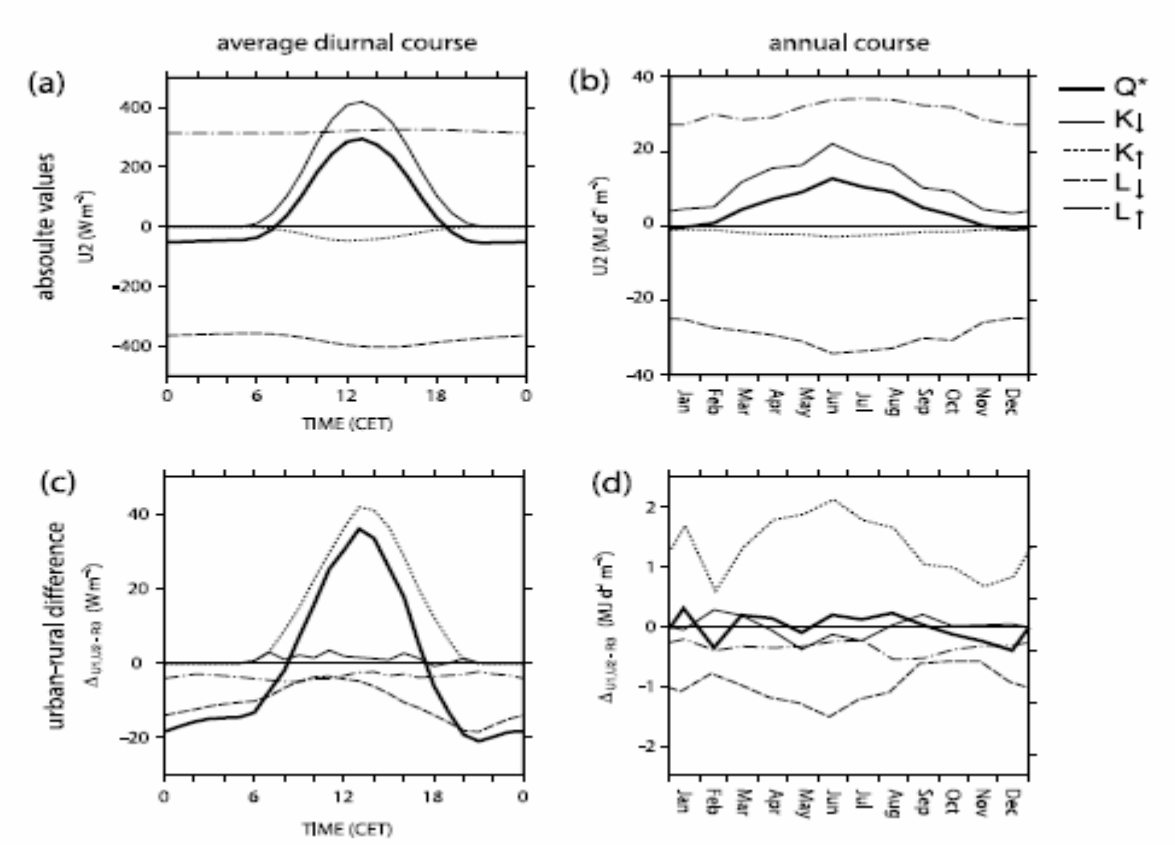

Figure 1, Daily variation (a) and annual variation (b) of the radiation balance components for the period September 2001 to August 2002 at an dense urban measurement site in Basel (CH). Differences of radiation components between two dense urban surfaces and one rural reference site in the daily variation (c) and annual variation (d) for the same period in Basel. Negative values indicate components with a relative energy loss from the city; positive terms are components where the city can achieve an energy surplus compared with the rural reference (Christen and Vogt, 2004).

Energy can be used to warm air, warm objects and fluids or evaporation of water, but also additional energy can be supplied through cooling of air, cooling of objects and fluids, condensation of water and anthropogenic energy use. The partitioning of these energy fluxes is described in the surface energy balance (Eq. 2):

Eq. 2 $$Q^* = Q_H + Q_E + \Delta Q_S + Q_F$$

The flux density of net all-wave radiation (Q*) is equal to the combined effect of sensible heat flux (Q_H), latent heat flux (Q_E), difference in urban storage heat flux density (ΔQ_S) and the anthropogenic heat flux density (Q_F).

Differences can occur between the energy balance in urban and rural surroundings. Reduced water availability in cities can reduce the amount of energy used for latent heat flux, while objects such as buildings can amplify the urban storage heat flux density. Due to human activity the anthropogenic heat flux density is higher in urban areas. This results in an increased sensible heat flux, and thereby higher temperatures (Figure 2).

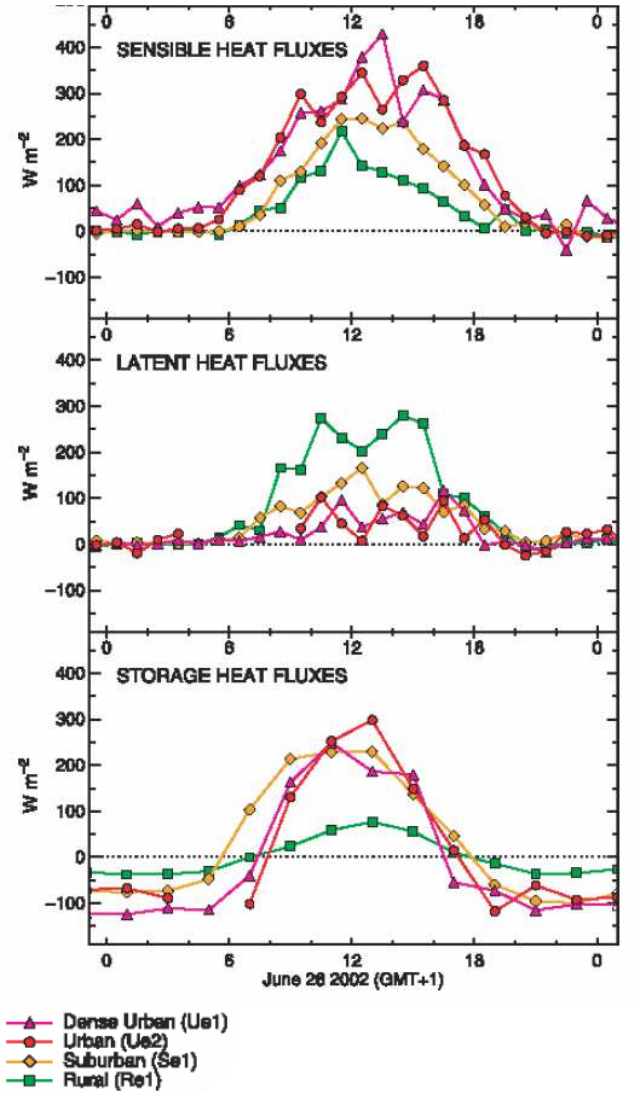

Figure 2, Diurnal cycles of sensible heat fluxes, latent heat fluxes and storage heat fluxes on June 26 2002 in Basel(CH) for four measurement location, two urban, one suburban and one rural location (Rotach et al., 2005).

Surface characteristics like albedo, aspect ratio, roughness length or moisture availability significantly control the energy balance partition (Christen and Vogt, 2004).The modified partitioning of the urban energy balance affects the whole boundary layer, its stability, thermodynamic properties and the mixing layer height. And finally, the modified urban energy balance results in typical urban climate phenomena like the urban heat island (Christen and Vogt, 2004).

As is visual in figures 1.a, 1.c and 2 there is a strong daily cycle for both the components of the radiation budget as for the components of the energy budget. The temperature differences between the city and the countryside is considered strongest during the night (Oke, 1982) . Also visible from Figure 1.b and 1.d is the annual cycle.

The differences between the different measurement stations in Basel indicate that there is a spatial variation within the city. Typical urban climate phenomena, like the urban heat island, are time and location specific (Arnfield, 2003, Oke, 1982).

1.1 Forecasting the UHI

Full scale measurements of the radiation and energy budget, as is done in Basel (CH) (Rotach et al., 2005, Christen and Vogt, 2004), give insight in the causes of temperature fluctuation in the city. However these measurements are costly and technical challenging, other methods have been presented to estimate the conditions of the urban boundary layer and the urban heat island. In this section we will examine indices used for the conditions of the urban boundary layer and the urban heat island.

The sky view factor and the aspect ratio of a street canyon are both features that have been proven to indicate the urban heat island (Svensson, 2004, Johnson and Watson,

1984, Unger, 2004) . Both are based on the alteration of the radiation budget by objects. The aspect ratio is the ratio between the height and width of streets and therefore is only applicable in homogenous conditions (Johnson and Watson, 1984). The sky view factor is the percentage of sky visible from a certain position and is often based on photographs or digital elevation models, which makes it better applicable in heterogeneous cases (Johnson and Watson, 1984).

Both parameters are based on the reduction of incoming radiation and increased transmission of longwave radiation by objects. Also the reduced albedo caused by the entrapment of (shortwave) radiation within urban canyons might be partially explained by these parameters. Low sky view factors are considered to be predictors of high nocturnal urban heat islands (Svensson, 2004). The relationship between the aspect ratio and urban heat island depends on the orientation of the street and the solar angle, overall higher aspect ratios are considered to be predictors of high nocturnal urban heat islands (Memon et al., 2010), however high aspect ratios might prohibit daytime heating and consequently strong nocturnal heat islands, resulting in a maximum nocturnal heat island with aspect ratios around 4[2] (Marciotto et al., 2010).

Because water availability has a strong influence on the urban energy balance, it might be expected that the surface fraction of water is a predictor of urban heat islands. Surface fractions of water do result in lower sensible heat fluxes, but water has a high storage capacity resulting in high nocturnal emissions of longwave radiation, which compensates the effects of increased latent heat flux (Hathway and Sharples, 2012, Robitu et al., 2006, Steeneveld et al., 2014, Theeuwes et al., 2013). The effect of cooling (due to moisture availability) is considered to be slightly smaller than the effect of nocturnal warming (due to high storage heat flux density) (Steeneveld et al., 2014). Although water bodies might not be a good indicator, water is still important. The fraction of impervious surface is claimed to be an indication for high nocturnal urban heat island because of the reduced water availability (Starke et al., 2010, Taha, 1997), while low vegetation surface fraction indicates high nocturnal urban heat island for the same reason (Bowler et al., 2010, Streiling and Matzarakis, 2003).

The anthropogenic heat flux is considered to be only present in urban areas. This heat flux is caused by all sorts of human activities, e.g. human metabolism, combustion engines, industrial activities, traffic. The total sum of the anthropogenic heat flux varies from <1 W/m2 in small towns with limited human activity and might be negligible (Bohnenstengel et al., 2013), to 200 W/m^2 in the large metropolis of Tokyo(Rizwan et al., 2008, Ichinose et al., 1999). In the midsize town of Basel (CH) the anthropogenic heat flux was 5 W/m^2 (Christen and Vogt, 2004). Relative to net all wave radiation (Q*) the anthropogenic heat flux might only be 2.5 % (Basel) or might be as large as 40 % (Tokyo) (Rizwan et al., 2008). The anthropogenic heat flux is difficult to measure, but the amount of human activity might be used as an indication for high nocturnal urban heat islands.

The specific properties of materials can be important for the subsequent storage of energy during the day and release at night, resulting in the nocturnal urban heat island. The heat capacity of water and urban objects can influence the amount of available energy (Myrup, 1969, Oke, 1982, Robitu et al., 2006). Materials with low thermal

2 Analyses is performed on a north-south oriented street in São Paulo, Brazil (23˚S), for the Netherlands this value might differ.

conductivity in urban surroundings are associated with high urban heat islands(Silva et al., 2010). Also, low emissivity of objects can result in high urban heat islands (Silva et al., 2010). Changing the albedo of objects and materials within cities is a proven mitigation strategy for the urban heat island (Oleson et al., 2010, Santamouris, 2012).

Research on the urban boundary layer have reviled that the urban heat island is strongest under conditions of low wind speed and low cloud cover(Morris et al., 2001, Oke, 1973, Stewart, 2000). With low cloud cover the difference between urban and rural temperature increases. In the situation of low cloud cover the difference in net longwave radiation is highest, because of the relatively high temperatures of urban objects compared to cold skies, resulting in high nocturnal urban heat islands(Morris et al., 2001, Stewart, 2000). During conditions of high cloud cover this difference becomes smaller.

In conditions of low wind speed the advection of (cold) rural air and turbulent mixing is limited resulting in stronger differences between urban and rural temperatures (Oke, 1973, Morris et al., 2001).

1.2 Measuring the UHI

Multiple studies all over the world have measured the urban heat island. In almost every major city in Europe, North America and East Asia heat island studies have been conducted (Stewart, 2011). Calculating the urban heat island is conducted using measurements of both in and outside the city.

The type of measurements results in some challenges for researcher. Due to heterogeneity of the city intra-urban variation of temperature are expected. The urban heat island seems to be the strongest during the night, which clearly indicate the temporal variation. Researches are often forced to choose which variation they will monitor, spatial or temporal. The spatial variation can be monitored using mobile measurement, but this results in limited measurement moment and thereby a limited insight in the temporal variation. Though, temporal variation can be monitored using stationary measurements over a longer time span, this only gives insight for a limited area (Stewart, 2011).

A way to monitor both temporal and spatial variation of temperature is to use multiple stationary measurements. In recent years measurement networks have been installed in multiple cities, although they give insight in the intra-urban variation, the density of the networks are often a lot smaller than the expected spatial variation of temperature.

The measurements density of some campaigns are 0.5 per km^2 in Basel (CH), 0.07 per km^2 in London (UK), 0.03 per km^2 in Phoenix, Arizona (US) and 1 per km^2 in Birmingham (UH) (Fast et al., 2005, Rotach et al., 2005, Watkins et al., 2002, Tomlinson et al., 2013).

1.3 Research Structure

In this research, we will investigate three aspects of the urban heat island in a small town in the Netherlands: Wageningen. First we will examine the intra-urban and temporal temperature variation of Wageningen, therefore we will use a network consisting of 30 measurement stations, this results in average density of 3 measurements per km^2. Second, we will investigate the causes of the temperature differences by constructing a statistical model. Third, we will examine projections of the

urban heat island in the years 2050 and 2100 by using the constructed model and climate scenarios.

First we will look at the spatial and temporal variation of the urban temperature and the urban heat island in Wageningen. This will give more insight in the urban heat island in small town in North West Europe. The possibility to look at intra-urban variation, with a measurement density of 3 per km^2 is unique in the world. The temporal differences of the urban heat island will be compared to measurements in other cities. Maps will be used to illustrate the spatial variation, while time series will be used to visualize the temporal variation.

Second, we will give more insight in the causes of the urban heat island by constructing and testing statistical models that can explain the urban heat island or the urban temperature. The models can in the future be used to estimate the urban heat island in Wageningen and possibly in other cities. The models will be constructed using multiple linear regression and will consist of a equation with multiple independent variables and coefficients.

Finally, the future urban climate will be examined. To do so, a transformation of current rural temperature to the future (Bakker and Bessembinder, 2012) will be combined with the statistical model. This results in the future urban temperature in 2050 and 2100. The future urban climate is important because of the combined effects of climate change and urban heat island. Only limited knowledge is available on the combined occurrence of these two phenomena and the presented method might be a quick way to estimate the future urban climate.

In the next chapter we will examine the methods and materials used to reach the output, In chapter 3 the results are presented and interpreted and we will end with the conclusions in chapter 4.

2. Method and materials

This chapter explains which methods and what materials are used to obtain the final results. As already explained this research consist of three parts, i.e. the temporal and spatial variation of the urban temperature, a statistical forecast model, and time series of future urban climate.

2.1 Measurements and basic calculations

2.1.1 Temperature measurements

A total of 30 weather stations were installed in and around Wageningen, just before the summer of 2013. The measurement campaign consists of the (meteorological) summer, i.e. the months June, July and August. The stations measure air temperature and relative humidity. They are located in different types of urban structures and are spread evenly over the city (red dots in Figure 4).

The measurement stations consist of a VP-3 Humidity/Temperature sensor (Decagon) located in a round 184 mm diameter shield, at the top of the shield a solar powered aspiration fan is located (Davis). The two solar panels for the aspiration fan are located on top the radiation shield and positions in a ±45˚ angle to the east and west. The solar panels were powerful enough to operate the fan, even in cloudy conditions. The positioning to the east and west extends the operational time in the morning and evening. The stations are attached to lampposts, to minimize the disturbance of the site. Because of the possible temperature interference with the lamppost (Watkins et al., 2002), The shield and solar panels were attached to on a 550 mm arm. The centre of the shield is positioned 460 mm from the lamppost at a height of 3 meter

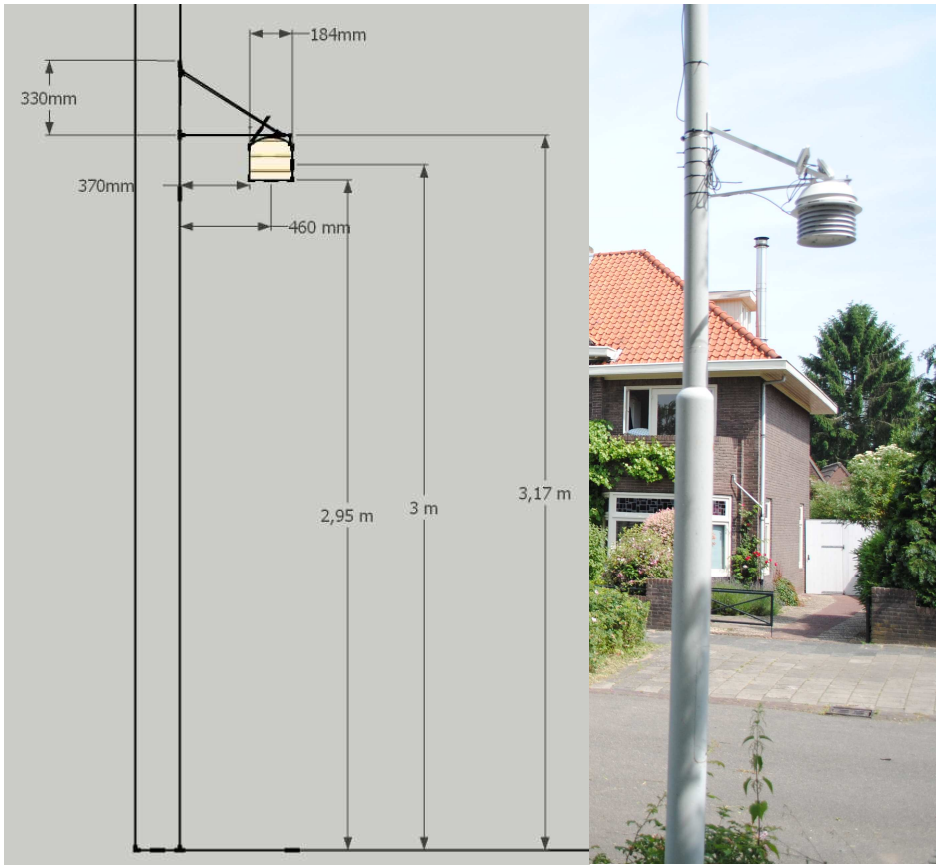

Figure 3, sketch of the measurement device attached to lamppost (left) and photograph of the device (right).

(Figure 3). The device is attached at a this height to prevent vandalism.

Averaged five minute data are stored on a ECMH20 data-logger (Decagon) and uploaded to the manufactures' website six times a day using a GPRS network.

Besides the 30 urban stations, two other measurement stations are used in this research (green dots in Figure 4), i.e. the previous and present measurement site of the meteorological department of the Wageningen University. This previous measurement site, named Haarweg (HW), is located approximately 500 meter westwards from Wageningen. The new measurement site, the Veenkampen (VK), is located 1.35 km west of the closest urban buildings and is used for multiple researches and international weather predictions. The Veenkampen will be used as a rural reference station during this research. At both locations measurements are performed in a Stevenson screen at a height of 1.5 meter above short grass land.

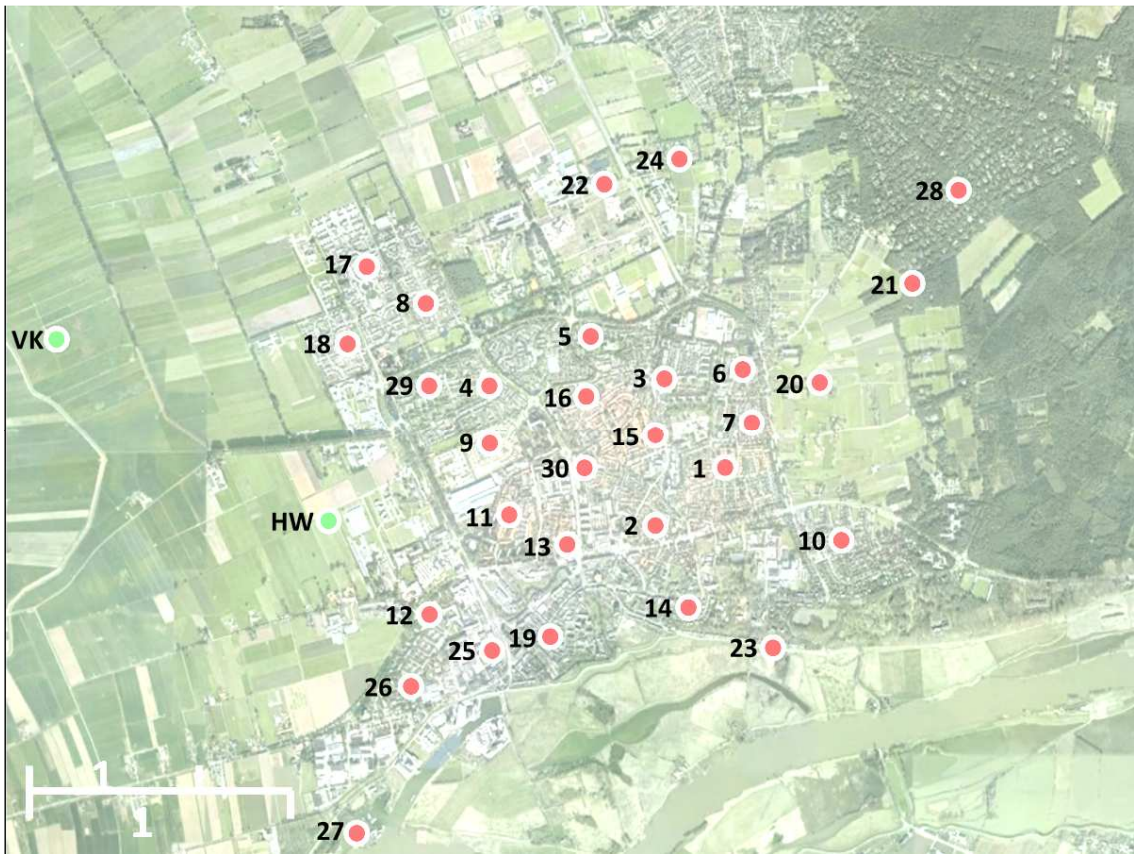

Figure 4, satellite image of Wageningen and the locations of the measurement stations. Green location have a Stevenson screen measuring at 1.5 m. The red location are attached to a lamppost at 3 m.

2.1.2 Altitude alteration

Because of differences in altitude within Wageningen and the small height difference between the two types of measurements all temperatures are adjusted for altitude. The temperatures are adjusted to a level of 5.5 meter above sea level which is the altitude of the Veenkampen rural reference station including the height of the measurement equipment. A standard lapse rate of 0.0098 K/m is used. The largest difference was 45 m, which results in a temperature difference of 0.44 K. This might look small considering normal temperature variations, but is relatively large considering the urban heat island, which ranges typically between 0 and 8 K.

2.1.3 UHI estimation

The urban heat island at any moment in time is the difference between the urban and rural temperature. For Wageningen, the Veenkampen location is used as rural reference station. Therefore, the urban heat island at every location can be described as[3]:

Eq. 3

$$UHI_{location} = T_{location} - T_{Veenkampen}$$

According to literature, the urban heat island will be the strongest during the night (Oke, 1982). To give insight in the maximum urban heat island the daily maximum was

[3] For calculations with regard to urban heat islands we used hourly averaged values.

selected. To ensure we are dealing with the nocturnal UHI only values between 18 UTC and 6 UTC (20 LT and 8 LT) are used. The maximum urban heat island is accounted for the previous day, so even if the maximum was reached at 2 June 02:00 it will be accounted as the urban heat island of 1 June.

Eq. 4 $$UHI\_max_{location} = \max(UHI_{location}) \qquad between\ 18\ utc\ and\ 6\ utc$$

Another expression of the daily urban heat island is the difference between the minimum temperature. These minima doesn't have to occur at the same time. Also the difference in minimum temperature will be attributed to the following night.

Eq. 5 $$Tmin_{location} = \min(T_{location}) \qquad between\ 18\ utc\ and\ 6\ utc$$

Eq. 6 $$UHI\_diffmin_{location} = Tmin_{Veenkampen} - Tmin_{location}$$

2.2 Temporal variation

To provide more insight in the temporal variation of the urban heat island in Wageningen, we will investigate temperature and urban heat island for a period of several days. We will use a period of time that represents calm and stable weather and compare the rural reference station Veenkampen and a measurement station in the old town centre.

2.3 Spatial variation

The spatial distribution of the urban heat island and the urban climate is visualized using the Matlab ScatteredInterpolant function. This function makes it possible to interpolate the values with three different interpolation techniques: linear, nearest neighbour, and natural interpolation. Extrapolation can be done with linear or nearest neighbour, but can also be disabled. This results in 9 different possible interpolation methods, which are all tested. To visualize the difference within the city we have interpolated the average summertime hourly urban heat island, the average maximum daily urban heat island, the average daily difference in minimum temperature and the average difference in the diurnal temperature range (DTR). The calculation of these terms are explained in the following section.

2.3.1 Testing interpolation method

To evaluate the interpolation methods as a predictor for the urban heat island we have compared interpolated values to real values. The interpolation was performed based on all available stations except one, the interpolated temperature at the grid point closest to that station is compared with the measured temperature.

2.3.2 Filter

Local fog and the passages of fronts can strongly influence the urban heat island, because these urban heat islands are not caused by the city a filter is used to exclude such cases. For daily values we have not used data with fog (minimum visibility lower than 1000 m) or rain (more than 3 mm cumulative precipitation)in the last 24 hour. For hourly values we have excludes cases with fog or rain in the last 16 hours.

The dataset consist of 91 days (2184 hours), of which 50 hours (1513 hours) where clear from rain or fog, while 41 days (671 hours) had conditions of rain or fog. 45% of the days where filtered out and 31% of all hours.

2.4 Statistical Model

The statistical relationship between the temperatures of the rural and the urban stations is investigated. Because there are 30 stations with different site specifications it is possible to test the importance of a number of urban morphological elements that might influence the urban temperature. The resulting model might be used to estimate the urban temperature in Wageningen or even in other cities. We will also formulate a statistical model for the daily maximum urban heat island and the daily difference in minimum temperature. As such, we will develop one model for hourly values and two models for daily values.

For the statistical models, a multiple linear regression approach will be followed. Hereby a linear model will be made where the coefficients are adjusted to represent a best possible fit. This will result in a formula in the following format:

Eq. 7 $$Y = \propto_0 + \propto_1 * X_1 + \propto_2 * X_2 + \propto_3 * X_3 + \ldots \propto_n * X_n$$

In this formula Y is the dependent variable, $\propto_n$ are the parameters that results from the regression, X_n are the independent variables and n is the number of independent variables. For the three regression to formulate, the dependent variable we will be the urban temperature, the maximum nocturnal UHI and the difference in minimum temperature. For the first regression, we will use filtered hourly data, while the other two are filtered daily values. As independent variable we might use site characteristics, meteorological conditions and radiation measurements. In the coming sections we will explain all possible independent variables.

The aim is to make a relatively simple model that is robust for practical use, therefore we will limit the amount of independent variables. Because of this construction, there will be multiple possible combinations of independent variables. All models will be validated using a split set up. Half of the observations (the odd days) will be used for constructing the model, while the other half of the observation (the even days) will be used to validate the model. For the selection of the model we paid special attention to some indicators within the validation process. First of all, we want the model and all coefficients to be significant ($P<0.05$). Secondly, the coefficients should have the same sign as in a 1 to 1 relationship between the dependent and independent variable. Further, we are looking for models with high level of explanation of variance (R^2-adjusted), low standard error (SE) and high index of agreement (d). All used indices are explained in Appendix III.

In the coming section all possible independent variables are explained. They can be categorized as non-location specific and location specific. We will first start with the non-location specific ones.

2.4.1 Diurnal Temperature Range

The Diurnal Temperature Range (DTR) is the difference between the maximum and minimum temperature during a day (Eq. 8). The difference between urban and rural temperature is largest during the night (Oke, 1982). This indicates the presence of a difference between the daily temperature range for these two locations, with lower DTRs for urban areas. According to Merkin (2004) a significant decreasing trend in the DTR has been observed in many urbanized regions.

The DTR will be used as an independent variable for the statistical model. Because the DTR is a daily value it will only be used for the models for the daily maximum urban heat island and the daily difference in minimum temperature.

Eq. 8 $$DTR_{location} = Tmax_{location} - Tmin_{location}$$

2.4.2 Rural Temperature

For the statistical model of the urban temperature we will use the rural temperature as an independent variable. Because the difference between the urban and rural temperature is small, and both have roughly the same trend, we assume that the rural temperature is an important predictor for the urban temperature. All temperature measurements are in degree Celsius.

2.4.3 Wind speed

Wind speed is important for turbulent mixing and processes of advection, multiple researchers have shown that high urban heat islands can be expected with low wind speeds. Conrads (1975) described a logarithmic-linear relationship between wind speed and urban heat island, Oke (1973) described a logarithmic-logarithmic relationship between the two, therefore we have tested not only wind speed but also the log of the wind speed. The nonlinear relationship might be explained by the influence of advection and turbulent mixing which already occur at small wind speeds and can strongly reduce the urban heat island.

Wind speed is measured at the Veenkampen rural reference station at a height of 3.44 meter, using a sonic anemometer. We assume there will be limited spatial difference over the Wageningen area. The wind speed is expressed in meter per second.

For the UHI_{MAX} and $UHI_{DIFFMIN}$ models we have used the average wind speed of the previous day, while for the urban temperature model we have used the average wind speed of the last 16 hours.

2.4.4 Radiation

From literature, we can understand that the radiation budget is important for the net flux density of all-wave radiation. Because of this theoretical link we have included different radiation terms as independent variable. For the daily models we have used the sum of the incoming longwave radiation, outgoing longwave radiation and incoming shortwave radiation in the previous day expressed as J/m^2, while for the hourly data the sum of the last 16 hours is used.

2.4.5 Antecedent Precipitation Index

During the summer of 2013, measurements of soil moisture are performed at different locations within the city. At 13 measurement sites the soil moisture was measured at the top layer (10-20 cm depth). Due to the exposure of the equipment the measurement couldn't be performed permanently. Therefore, every 7 to 14 days measurements were performed for a short period of time at 2 locations close (<5m) to the measurement site. Due to malfunctioning of the equipment some data were lost while at other location the spread of the soil moisture content was large. Because of the limited quality of the data it was decided to not use the observed soil moisture content directly, instead we have used the antecedent precipitation index (API) as a proxy for soil moisture (Eq. 9).

Eq. 9

$$API_t = API_{t-\Delta t} * k + P_{\Delta t}$$

The API at time step t (API_t) is constructed based on the API of the previous time step ($API_{t-\Delta t}$) multiplied by a regression coefficient(k) and added with the precipitation during the time period ($P_{\Delta t}$). This index is used for the description of water in both river catchment areas (Fedora and Beschta, 1989) and soil moisture (Jackson, 1993, Blanchard et al., 1981). The regression coefficient depends on the flow rate, which in the case of the catchment is area depends, while in the case of the soil moisture depends amongst other on soil type and aquifers.

A regression coefficient of 0.95 has been chosen because of a good fit with the found soil moisture contents (Figure 5).

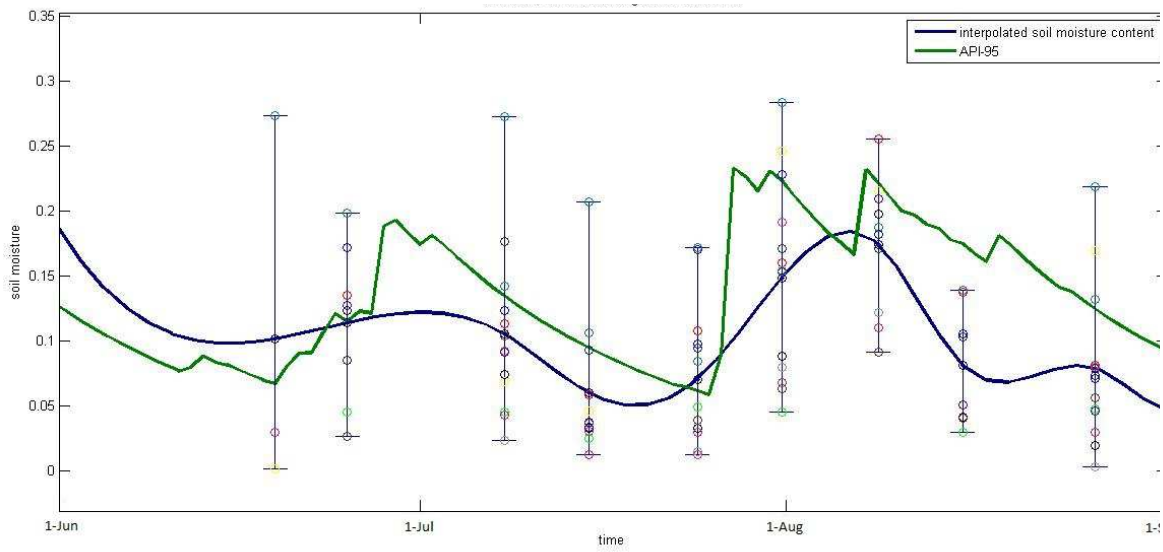

Figure 5, the average measured soil moisture content (spheres), the interpolated soil moisture content based on the average measurements (blue line) and the (rescaled) API with regression coefficient of 0.95. The error bars stretch from the minimum to the maximum found soil

2.4.6 Cloud cover

The amount of cloud cover influences the radiation budget, since clouds have a relatively high temperature compared to clear skies, more longwave radiation is re-emitted to the surface. In the absence of clouds the urban heat island becomes larger, a large difference occurs for incoming longwave radiation, because of the large difference between the cold clear skies (low emissions) and warm objects (Morris et al., 2001).

Because cloud cover is not measured at the Veenkampen we will use cloud cover measured at the KNMI measurement site at Deelen, 17 km north east of Wageningen. The cloud cover will be expressed in octas. We assume differences in cloud cover are small compared to effects by the other variables.

The following independent variables are specific for every location.

2.4.7 Surface fractions

Of all measurement sites surface percentages (built, vegetated, paved, open, water and impervious surface) in the direct 20 meter have been estimated based on visual appearance.

2.4.8 Sky View Factor

The SVF is the percentage of sky that is visible from a certain location. A canon digital camera with fish eye lens is used to make sky view photos. Sky view photos are limited to a specific location, while the measured temperature is expected to represent a larger area. Therefore multiple photos are taken at all the locations. One photo is taken at the street side of the station, one at the middle of the street at the level of the station, two others are taken at the middle of the street approximately 10 to 15 meters away from the station. At non-uniform locations additional photos were taken.

The SkyViewFactorCalculator is used to calculate the sky view factor for every photo. The program is developed by the Urban Climate research group of the University of Gothenburg, based on papers of Holmer et al. (2001) and Johnson and Watson (1984). For every location the average sky view factor of the 4 to 6 photos is used. It is assumed that this averaged values gives a good representation of the situation.

2.4.9 Incoming shortwave radiation within the city

The program Rayman 2.0 (Matzarakis et al., 2010) is used to estimate the incoming shortwave radiation within the canyon taking into account the obstruction of direct radiation by objects. To do this the radiation measured at the Veenkampen is combined with Sky View Photos. The multiple photos per location results in multiple time series of radiation per location. These values are averaged and form an indication of the radiation in the direct surroundings of the measurement site.

2.4.10 Normalized Difference Vegetation Index

Normalized Difference Vegetation Index (NDVI) is a relatively simple graphical indicator of live green vegetation, often used for the analyses of satellite images. The NDVI is calculated as follow:

Eq. 10

$$\mathrm{NDVI} = \frac{\mathrm{NIR} - \mathrm{VIS}}{\mathrm{NIR} + \mathrm{VIS}}$$

in which NIR is the spectral reflectance measurement acquired in the near-infrared spectrum and VIS is the spectral reflectance measurement in the visible spectrum (Huete et al., 2002). The reflectance in the different spectral bands is depending on properties of the surface. Which results in a high $(\rightarrow 1)$ NDVI for vegetation, a neutral (0) NDVI for bare soil and buildings, and a negative $(\rightarrow -1)$ NDVI for water.

The NDVI has been made available by the website groenmonitor.nl (Figure 6). During the summer months, a total of 8 satellite images have become available for the Wageningen area. The spatial resolution of the satellite images is 25 meter. An average NDVI is calculated for every location based on the NDVI in a radius of 200 meter around the measurement site. The values are interpolated over time using a spline interpolation method.

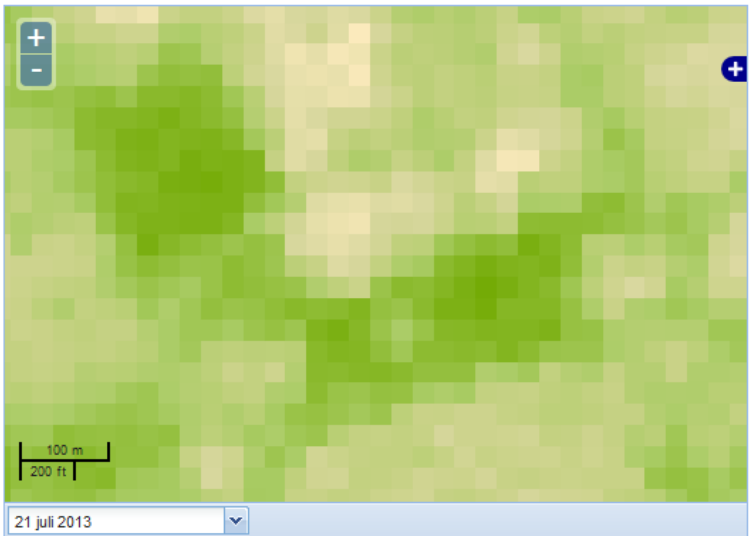

Figure 6, example of visualization used by http://www.groenmonitor.nl. The greener the area the higher the NDVI.

2.5 Future urban climate

In the previous part we have formulated a statistical model which can estimate the urban temperature. This model will be used to provide insight in the future urban climate. Instead of using present day data we will use future data that will be based on a climate transformation.

In 2006, KNMI presented climate scenarios based on members of a combined global and regional climate model (van den Hurk et al., 2006). Four different types of climates were visible in the climate models, resulting in four different climate scenarios. It consist of an increase in temperature of 1 K or 2 K (2050 climate compared to 1990 climate) and a general circulation pattern similar to the present day situation, or a change in these circulations patterns. (Table 1). Based on these climate scenario a transformation tool is constructed (Bakker and Bessembinder, 2012).

Table 1, KNMI'06 climate scenarios

G	Temperature rise of 1 degree on earth in 2050 compared to 1990, with no change in air circulation patterns in Western Europe.
G+	Temperature rise of 1 degree on earth in 2050 compared to 1990, with milder and wetter winters due to westerly winds, and warmer and drier summers due to more easterly winds.
W	Temperature rise of 2 degree on earth in 2050 compared to 1990, with no change in air circulation patterns in Western Europe.
W+	Temperature rise of 2 degree on earth in 2050 compared to 1990, with milder and wetter winters due to westerly winds, and warmer and drier summers due to more easterly winds.

2.5.1 Temperature transformation

Based on the four climate change scenarios, Bakker and Bessembinder (2012) built a transformation tool that can transform historical time series of temperature into a future one. The transformation tool is based on the change in temperature according one of the

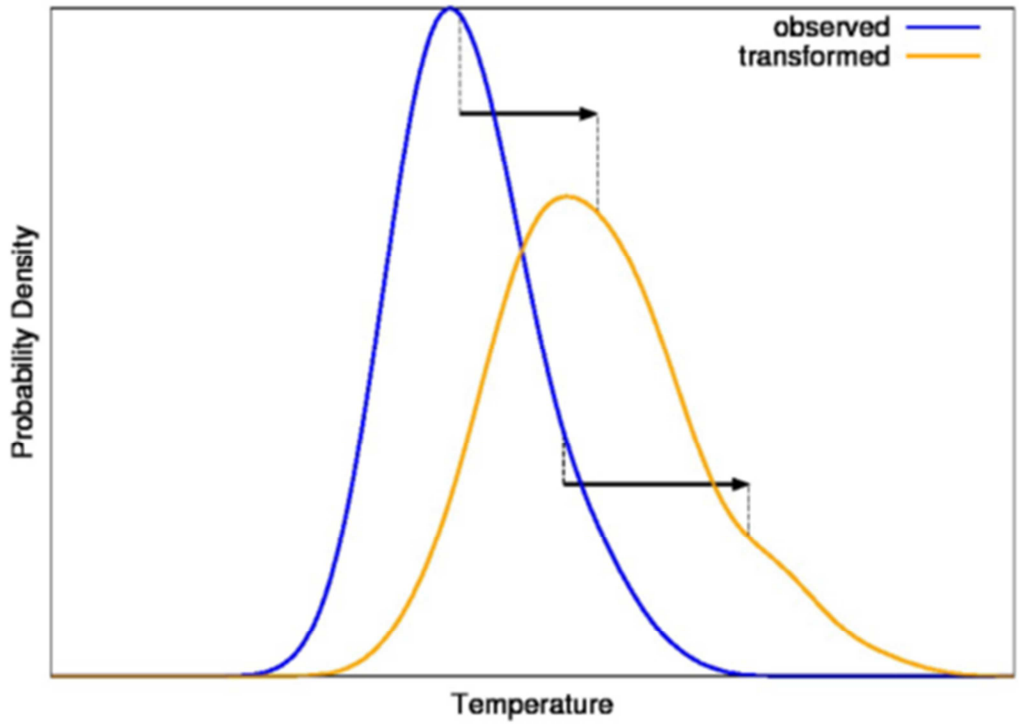

Figure 7, Visualisation of the transformation tool

four scenarios and the assumption that the probability of occurrence changes unevenly for different percentiles. The change for high percentiles is larger than for low percentiles. This results in a shift in the probability density for temperatures, the curve becomes flatter and wider (Figure 7). For each scenario and each month change factors are given for the 10^{th}, 50^{th} and 90^{th} percentile, all other percentiles have a change factor that is interpolated or extrapolated based on these 3 values. The temperature in the future time series is constructed based on the historical time series and the change factor. The original transformation tool was designed for daily values, while for this research we are working with hourly data. To convert the daily transformed values to hourly values a conversion factor is constructed for every day and applied on every hour of that day.

To construct a future rural temperature time series for the Wageningen area, the transformation tool is applied on data from the Haarweg and the Veenkampen. Because the Veenkampen is only operational since 2012 no historical data of the 1990 climate is available at this location, therefore the historical data of the Haarweg is used. The change factors are based on historical measurements at the Haarweg measurement location between 1976 and 2005. The change factors are applied to the Veenkampen temperature of summer 2013, hereby a future time series of temperature is constructed in which the conditions are comparable with the 2013 case accept for the temperature increase due to climate change. There is a small bias between the 1990 climate and the 2013 summer measurements that might result in change in the in constructed future climate. We take this bias for granted, because it is our goal to represent a future time series taking into account climate change, and this change will still be visible.

A full mathematical description of the transformation tool can be found in Appendix IV.

3. Results

In this chapter, we describe our results. We will use the same structure as in previous chapters, so we will first study the temporal and spatial variation of the urban heat island, second the statistical model will be examined and finally the future time series, taking into account climate change, will be discussed.

3.1 Temporal and spatial variation

3.1.1 Temporal variation

To investigate the temporal variation of the urban heat island we will examine the period from 14 to 21 July 2013. In this period a high pressure area is moving from the Atlantic ocean towards the British Isles, where it becomes stationary the British Isles, a secondary high pressure system is visible over central Europe. Low pressure areas are active to the North, especially over Iceland, and a minor low pressure system is visible over central Spain (Figure 9). During the entire week the pressure gradient above the Netherlands is small, but the predominant flow is coming from the South.

Two stations will be examined to investigate the temporal difference during this period (Figure 8). The rural reference station Veenkampen (VK) is located in a flat open grassland, the area is relatively wet because of the presence of peat in the area (Figure 10). A small stream is located a few meter to the west. The urban measurement site is

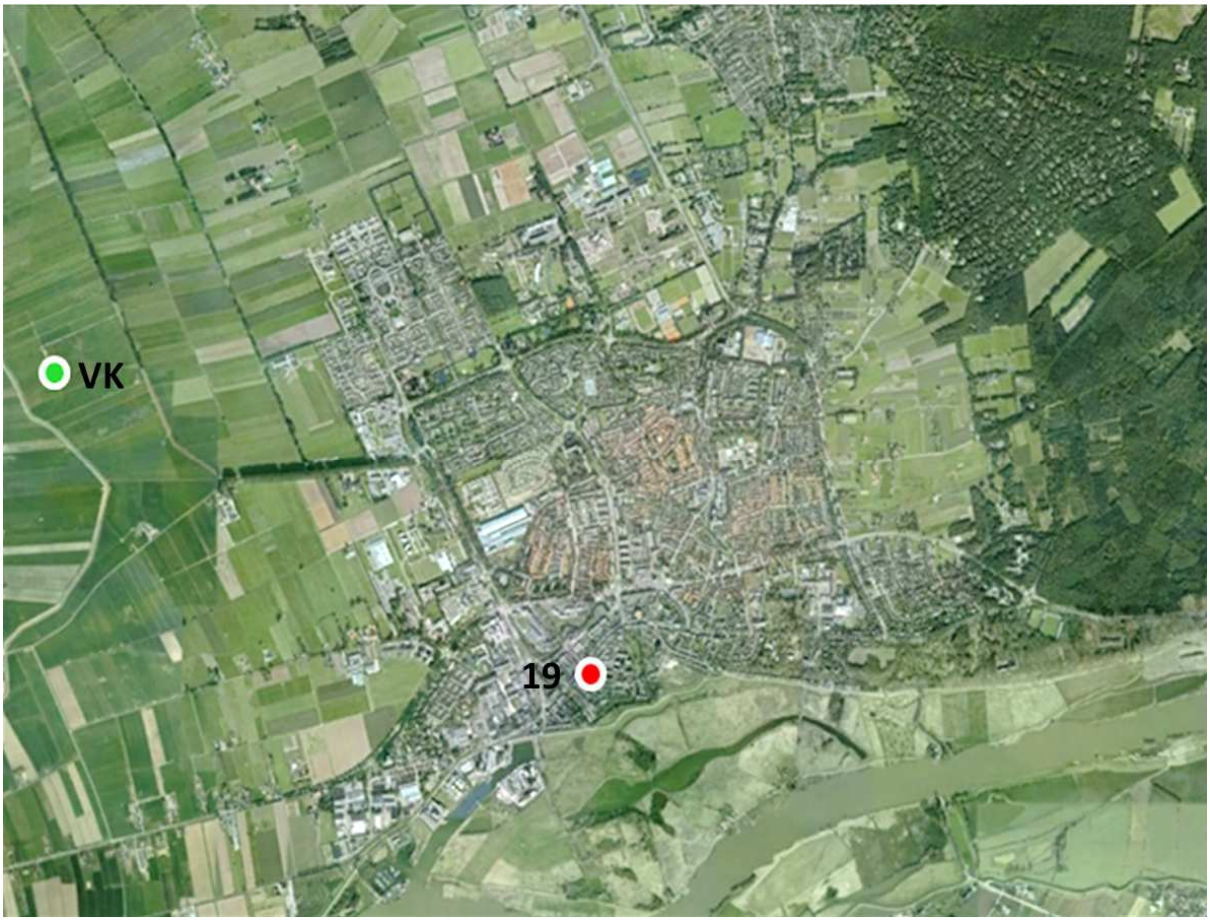

Figure 8, relative location of the two measurement locations. The distance between the stations is approximately 3.5 km.

located at the Markt (19), which is the old town centre square. A church is located in the centred of the square, while traditional 3 to 4 story houses enclose the square. A few trees are the only vegetation in the closest 100 meter, while the square is paved with traditional clinker pavement (Figure 10). The Markt has on average the strongest urban heat island, thereby an ideal showcase to examine the temporal variation of the UHI.

Figure 10, the left picture shows the Stevenson screen located at the Veenkampen measurement site. The right is taken from the measurement site at the Markt, showing the church, in the background the traditional houses, that enclose the square, are visible.

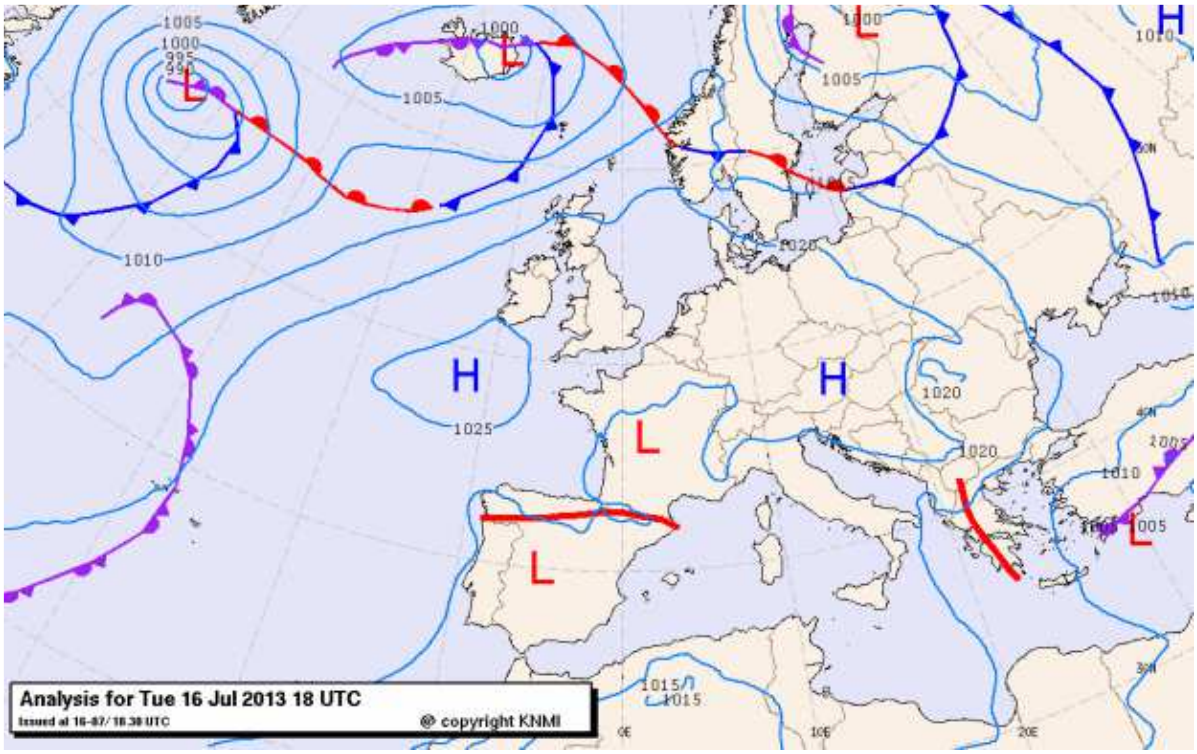

Figure 9, analyses for Tuesday 16 July, 18 UTC by the KNMI. The High pressure area southwest of England is moving slowly to the northeast. The other high pressure area depicted above Austria is shifting rapidly. The low pressure area above France is filled up within 2 days, while the lows above Iceland and Spain are more stationary and permanent during the entire week.

During the period of 7 days the temperature difference from 10 ºC at night to almost 30 ºC on 18 July in Wageningen. All days have a maximum temperature above 20 ºC, 5 days are above 25 ºC. At the rural station the minimum temperatures are all under 15 ºC except during the night between 19 and 20 July. The urban temperature is higher at almost every time, with a clearly visible higher maximum temperature of approximately 2 ºC. The minimum temperature at the urban site is considerably higher than the rural minimum temperature. The difference between the two location is fluctuating between 0 and 5 ºC, with a maximum during the nights (around 4:00 UTC), and a minimum a few hours later around 7:00 UTC.

Overall there is a difference between the maximum temperature, but also a difference between the cooling rate at the two locations (Figure 11). The combined effect of these two differences results in the maximum urban heat island to occur during the night, just before the end of the night. During the 19th of July and the following night there was considerably more cloud cover. The UHI during this day is completely different than the other days, with an absence of a strong maximum at night. Compared with the other days the difference during the maximum temperature is of similar size, but the night-time cooling at the rural station is strongly reduced. At both locations the night-time cooling is comparable for this night.

The presents of clouds might have reduced the cooling capacity of the rural measurement station. The cooling rate of the urban site is always lower, because of the presents of buildings and objects, resulting in an nocturnal urban heat island.

An urban heat island of 5.8 ºC is found during the night between 20 and 21 July, being the strongest of this time period. On average the urban heat island during this period was 2.41 ºC, with an average maximum urban heat island of 3.98 ºC, if the July 19th is not taken into account because of the presents of cloud cover, the maximum urban heat island is considerably larger, 4.32 ºC.

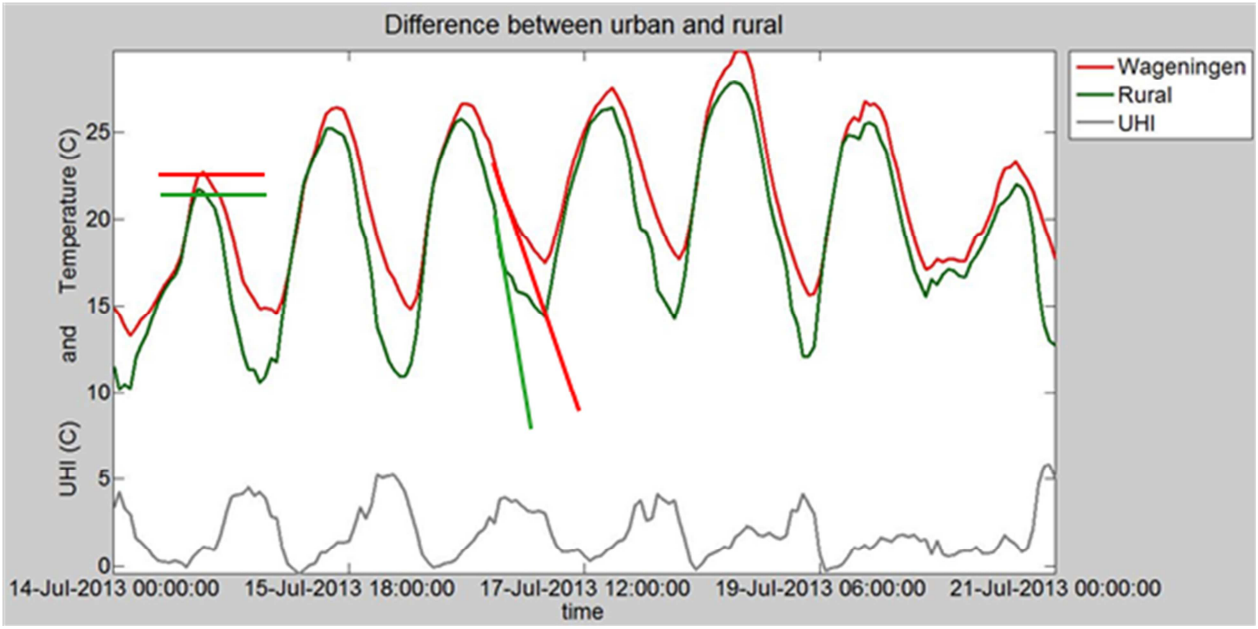

Figure 11, time series of the Wageningen (location Markt) and the rural temperature during the period 14 July 0:00 UTC and 21 July 0:00 UTC.

3.1.2 Spatial variation

To examine the spatial variation of the urban heat island in Wageningen the Matlab ScatteredInterpolant function is used. For all shown results a linear interpolation, without extrapolation is used. This method had the best fit between interpolated and real values. With all methods of extrapolation unrealistic values are generated at the outer regions of the plot because of the absence of reference stations in close proximity. To visualize the location of the plot, contours of the built area of Wageningen and Wageningen-Hoog are plotted, as is the contour of the Rhine river. Also the locations used for the interpolations are displayed (blue dots). At some moments the Haarweg location is not used, because of too much missing values, also one location is the north west of Wageningen is not always used because of long time series of missing values.

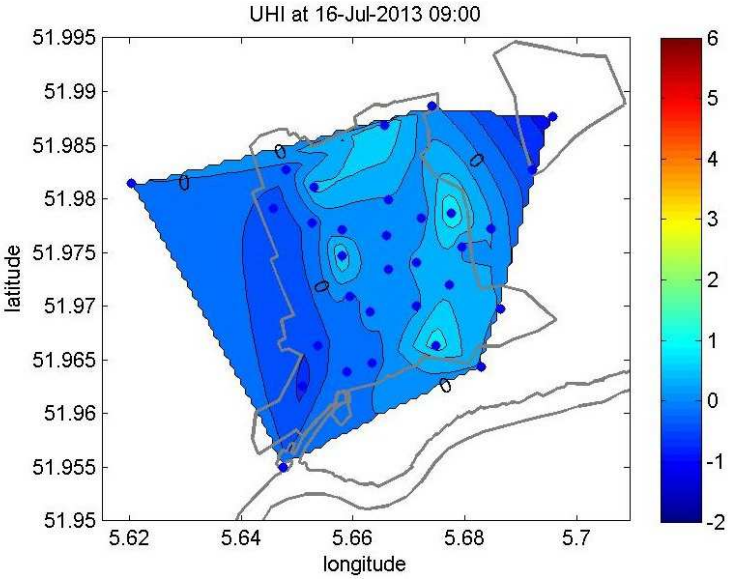

Figure 12, the urban heat island at 16th of July on 9:00 UTC.

The spatial variation at the morning of 16th of July is displayed in Figure 12, at that moment the urban heat island has an minimum for almost every location. An UHI of approximately -1 ˚C is visible in Wageningen-Hoog and one of approximately -0.5 ˚C in the West of Wageningen. the urban heat island in other areas are also close to 0 with a maximum of 0.67 ˚C. The centre of Wageningen is considerably warmer than the even at this moment.

A similar plot can be made for a period of maximum urban heat island (Figure 13). On the 20th July at 23:00 UTC a maximum is reached at the Markt, the temperature difference between the Markt and the Veenkampen is at that moment 5.8 ˚C, but also other location are considerably warmer. The southern part of Wageningen is warm, with urban heat island higher than 4 ˚C for reasonable large area, although part of these high urban heat islands are caused by extrapolation of the values. Also a residential area in the Northwest is remarkably warm. In-between Wageningen and Wageningen-

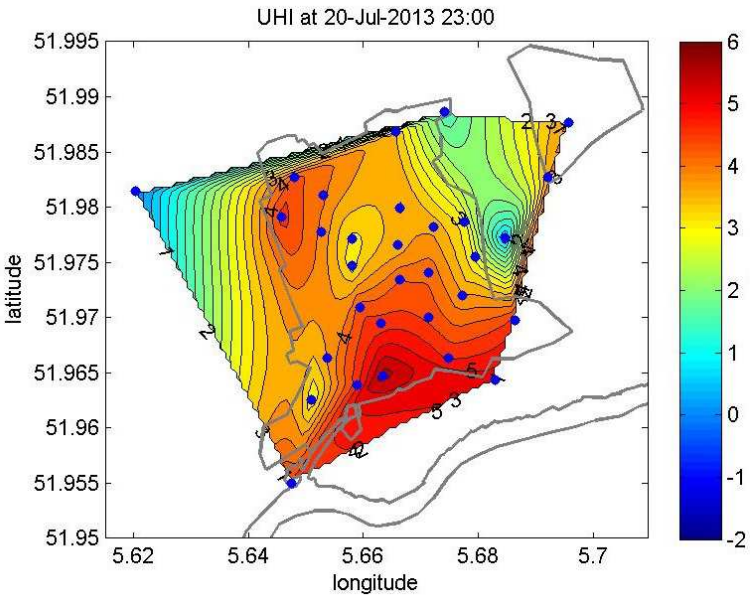

Figure 13, the urban heat island on 20th July at 23:00 UTC.

Hoog the temperature is only 1.4 ºC higher than the Veenkampen, Therefore the urban heat island has a reasonable match with the contours of both towns.

Both Figure 12 and Figure 13 show extreme cases for positive and negative urban heat islands. If we would look at average values over the entire summer we have a somewhat more moderate view. Figure 14 shows the average maximum UHI for the summer, for the selected days with rain or fog are not taken into account[4]. The spatial distribution is similar as in Figure 13, with highest urban heat island found in the southern part of the town and a secondary warm location at the north-west. Also the difference in minimum temperature (Figure 16) has the same spatial distribution, but the values are somewhat lower. Some locations reaching an average of 4.5 ºC for the daily maximum UHI, while the difference in minimum is not higher than 3.3 °C. Steeneveld et al. (2011) found an average daily maximum UHI of 1.8 °C in Wageningen, the used location is marked in Figure 14 with a blue star. This research was based on measurements by hobby meteorologists over an period of 2.5 years, with a total of 826 used days. The location is in the zone that resembles an average UHI of 3.75 to 4.0 ºC. The difference between the two measurements might be explained by the research period: we have only used data gathered in the 2013 summer months, while Steeneveld et al. (2011) used 2.5 years of data both from all seasons.

If we look at the average temperature of the entire summer (Figure 15) we see that the contours of the city have a good fit with the temperature profile. The spatial differences are smaller than considering both definitions of the UHI, only a maximum of 1.5 ºC difference, this has to do with the reduced UHI during the day.

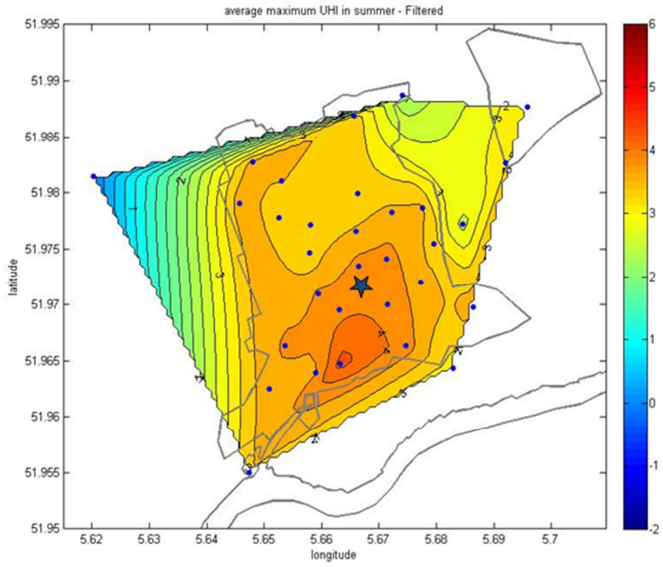

Figure 14, the spatial distribution of the average maximum UHI during the 50 summer days without disturbance of rain or fog. The blue dots represent the used measurement sites, the blue star is the location of the hobby meteorologist used by Steeneveld et al. (2011).

[4] The filter had removed 41 days, resulting in a sample size of 50 days.

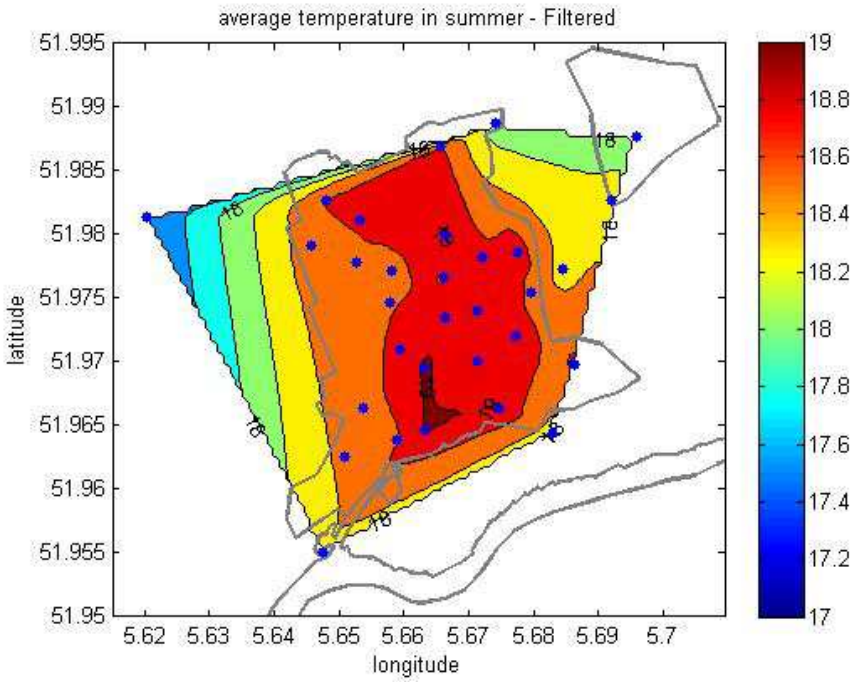

Figure 15, the spatial distribution of the average temperature during summer days with clear conditions.

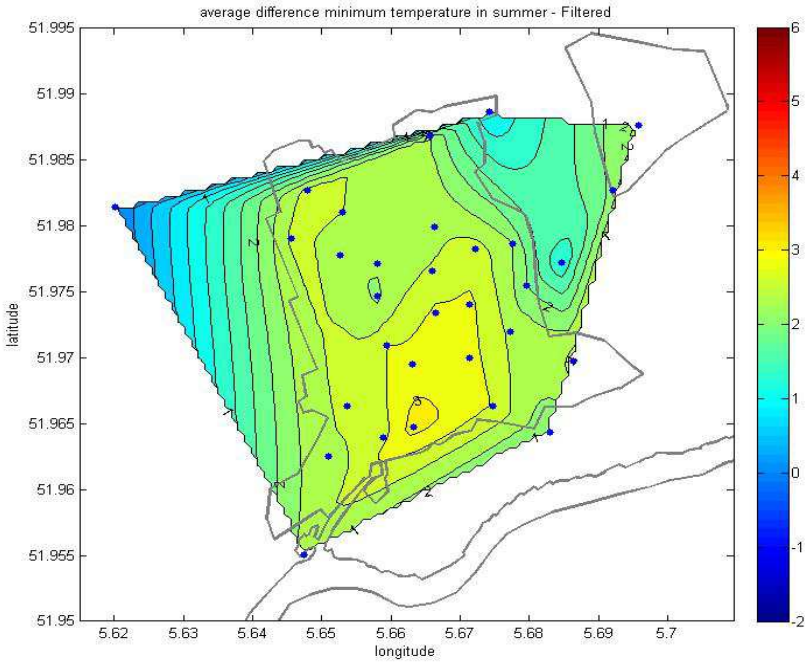

Figure 16, spatial distribution of the average difference in minimum temperature. Also filtered for conditions without rain or fog.

3.2 Statistical model

The spatial resolution of temperature measurements in Wageningen is unique, with 3 measurements per square kilometre it is far higher than comparable measurement campaigns around the world. Through the high density measurements we can investigate which aspects are important for the occurrence and strength of the urban heat island.

By using the temperature measurements at all 30 stations and gathering additional information about the locations we have the opportunity to investigate the causes of the urban heat island. The statistical model will indicate which variable, or combination of variables, are statistically important for the urban heat island.

We have focused on three different dependent variables, the daily maximum urban heat island, the difference in minimum temperature and the urban temperature. In the following sections we will examine them independently. We will begin with the daily maximum urban heat island.

3.2.1 Daily maximum UHI

For this statistical model we have used 50 days of data, the other 41 had conditions with rain or fog which were filtered out. 26 of the 50 days (the odd days) where used for the regression, while the remaining 24 (even) days were used to validate the model. Because of the large number of tested independent variables (17) the possible combinations of variables was enormous. To minimize computing time and to keep the model simple, only the possibilities with 1, 2, 3, 4 or 5 independent variables were constructed and validated, this resulted in approximately 18.000 statistical models. Based on the selection procedure we finally selected the model described in Eq. 11.

Eq. 11

$$UHI_{max} = 0.1737 * DTR - 1.238 * log(u) - 0.08168 * API - 2.733 * NDVI + 0.006200 * Imp + 2.474$$

The independent variables used in this statistical model are the Diurnal Temperature Range (DTR) of the preceding day measured at the rural reference station, the logarithm of the average horizontal wind speed at 2 meter high (log(u))of the proceeding day, the Antecedent Precipitation Index (API) which in itself is a daily value, the NDVI as constructed at 12:00 UTC[5], and the estimate impervious surface fraction in a 20 meter radius around the measurement site. The DTR, the wind speed and the API are constant for the entire city, while the NDVI and the impervious surface fraction differ for every location. The first four variable fluctuate in time, while the surface fraction is constant during the entire summer.

Table 2, statistical parameters for the model describing the daily maximum urban heat island.

N	717
R2 -adjusted	0.2365
Index of agreement	0.7116
RMSE (˚C)	0.9936
RMSEs (˚C)	0.6909
RMSEu (˚C)	0.7141

The model is valid on within the range depicted in Table 3.

[5] The NDVI changes during the summer, spline interpolation technique was used to fill in missing data, thereby hourly data was produced. For this model we have used the 12:00 UTC NDVI because we believe it is representative for the entire day, also because the fluctuation in NDVI are minimal.

Table 3, range of variable (Eq. 11).

Variable	Min.	Max.
DTR	2.3	15.8 (◦C)
u	0.2	10.1 (m/s)
API	0	30.5 (mm)
NDVI	0.25	0.78
Imp	7.5	100 (%)

This model unfortunately does not show the highest explained variance of all tested models, but the found coefficients, for this model, are in line with theory and with findings in this research (not shown). The statistical parameters for this model are presented in Table 2. A total of 717 samples were used, which is approximately 24 days at 30 locations. The adjusted R2 is low, while the index of agreement (d) is somewhat better. This indicates that the variance (R2) of the urban heat island is not particularly good described by the model, while the relative size of the error (d) is reasonable. The Root Mean Square Error (RMSE) is relatively large, but striking is the fact that a large proportion of this error is systematic (RMSEs), indicating that an additional independent variable might have been needed for better explanation of the daily maximum UHI.

3.2.2 Difference in minimum temperature

For the construction of the model for the difference in minimum temperature the same data is been used as for the model for daily maximum UHI, both are daily values. Also for this dependent variable only models with 5 or less independent variables are tested, also resulting in ±18.000 models. The chosen model is expressed in Eq. 12. The log(u), API and NDVI are the same as explained for the previous model, but paved refers to the estimate paved surface fraction (only valid in the range displayed in Table 5).

Eq. 12

$$\mathrm{UHI}_{\mathrm{diffmin}} = -1.101 * \log(u) - 0.07793 * \mathrm{API} - 2.178 * \mathrm{NDVI} + 0.01151\ \mathrm{Paved} + 3.340$$

Remarkably is the fact that models with DTR as independent variable were not better, indicating that the effect of temperature range is minimal with respect to the difference in minimal temperature.

The explained variance is low, with only 12.45% being explained. The index of agreement is somewhat higher than the explained variance, but also considerable lower that for the previous model. The RMSE is around 1.1 ˚C which is relatively high (Table 4). Also for this model a large part of the error is systematic, indicating that an additional independent variable might have been better. This is interesting, because the model only consist of 4 variables, while also models with 5 have been tested. This indicates that none of the tested independent variables would increase the performance of the model without violating the pre-set conditions[6]. This might be caused by the fact that the minimum temperatures doesn't have to occur at the same moment, under normal conditions the minimum temperature at the urban site is reached later than at the rural site, this time lag is approximately 1 h. The time lag is the result of objects prohibiting radiation to

Table 4 statistical parameters for the model describing the difference in minimum temperature.

N	717
R2 -adjusted	0.1245
Index of agreement	0.5391
RMSE (˚C)	1.1152
RMSEs (˚C)	0.9935
RMSEu (˚C)	0.5031

[6] All model should be significant (P<0.05) and the sign of the coefficients should be the same as in a 1:1 relationship with the dependent variable.

Table 5, range of variable (Eq. 12).

enter the street canyon, this would imply that that the model would be better if it was solely based on locations without object in the eastward direction (e.g. east-west oriented streets), however this is not tested.

Variable	Min.	Max.
u	0.2	10.1 (m/s)
API	0	30.5 (mm)
NDVI	0.25	0.78
Paved	7.5	60 (%)

3.2.3 Urban Temperature

The model for urban temperature is based on hourly values of all 30 stations, during the entire summer 1513 hours passed the filter. Again, the hours of the odd days (810 hours) are used to construct the model, while the hours of the even days (703 hours) where used to test the model. Because the DTR is a daily value, this couldn't be used for this model, therefor we have used the rural temperature. For most variables we have used the average or sum in the preceding 16 hours instead of 24 hours in the two previous models. Again 17 independent variables are tested in combinations of 1 to 5 variables per model resulting in 18.000 tested models, while the chosen model is displayed in Eq. 13. T_{urban} is the hourly temperature at the 30 urban locations, T_{rural} is the hourly temperature at the rural reference station Veenkampen, log(u), API and NDVI are already explained, while Radurban is the constructed sum of the incoming shortwave radiation at the 30 locations (valid in the range displayed in Table 6). The first three variables only fluctuate in time, while the last two fluctuate in space and time. Because the urban and rural temperature result in the urban heat island (Eq. 3) we can rewrite Eq. 13 to Eq. 14 resulting in a formulation of the hourly UHI. The coefficients found are all in line with found relationship between the UHI and the individual independent variables as is visualized in Appendix VI.

Table 6, range of variable (Eq. 13).

Variable	Min.	Max.
Temp	2.2	33.9 (◦C)
u	0.2	10.1 (m/s)
API	0	30.5 (mm)
NDVI	0.25	0.78
Rad	$5.5e^{6}$	$2.8e^{7}$ (J/m^2)

Eq. 13

$$\mathrm{T_{urban}} = 0.9765 * T_{rural} - 0.8204 * log(U) - 0.02312 * API - 2.365 * NDVI + 2.392\mathrm{e}-08 * Rad_{urban} + 2.706$$

Eq. 14

$$UHI = \mathrm{T_{urban}} - 0.9765 * T_{rural} = -0.8204 * log(U) - 0.02312 * API - 2.365 * NDVI + 2.392\mathrm{e}-08 * Rad_{urban} + 2.706$$

In contrast to the previous two models the results indicate that the model has a good fit with the found results. More than 97% of the variance in urban temperature is explained by the model, while the index of agreement is even higher than 99%, indicating that there is only a relatively small error. The RMSE is only 0.8867 ˚C which is small compared to the average temperature of 18.4 ˚C. Only 0.1855 ˚C of the RMSE is systematic, so there is little room for improvement of the model (Table 7).

Table 7 statistical parameters for the model describing the urban temperature.

N	24151
R2 -adjusted	0.9716
Index of agreement	0.9927
RMSE (˚C)	0.8867
RMSEs (˚C)	0.1855
RMSEu (˚C)	0.8466

3.3 Future Temperature

Based on the temperature transformation described by Bakker and Bessembinder (2012), the future temperature at the Veenkampen is been constructed. Figure 17 shows the temperature between 14 and 21 July transformed to a 2050 and 2100 climate for both scenario G and W+. The G scenario shows an increase slightly more than 1 °C in 2050 and 2 °C in 2100, which agrees with the description of the scenario. Contrary, the W+ scenario shows an increase in temperature of approximately 4 °C in 2050 and 8 °C in 2100, which is more than described in the scenario. In the W+ scenario, the temperature should increase by 2 °C in 2050 compared to 1990, but due to changes in general circulation the summer months are warmer and dryer. The change factor for the 90th percentile in July is 3.67 °C (Appendix V, Table 10), which is close to the 4 °C found. July 2013 was relatively warm, being the 8th warmest July month ever recorded in De Bilt (Weerstatistiek) . Hence, the resulting temperature in the W+ scenario seem to be higher than expected, but the results are in line with the transformation tool. Both transformed time series based on the G+ and W scenarios (not shown) are also in line with expectations from the climate change scenarios.

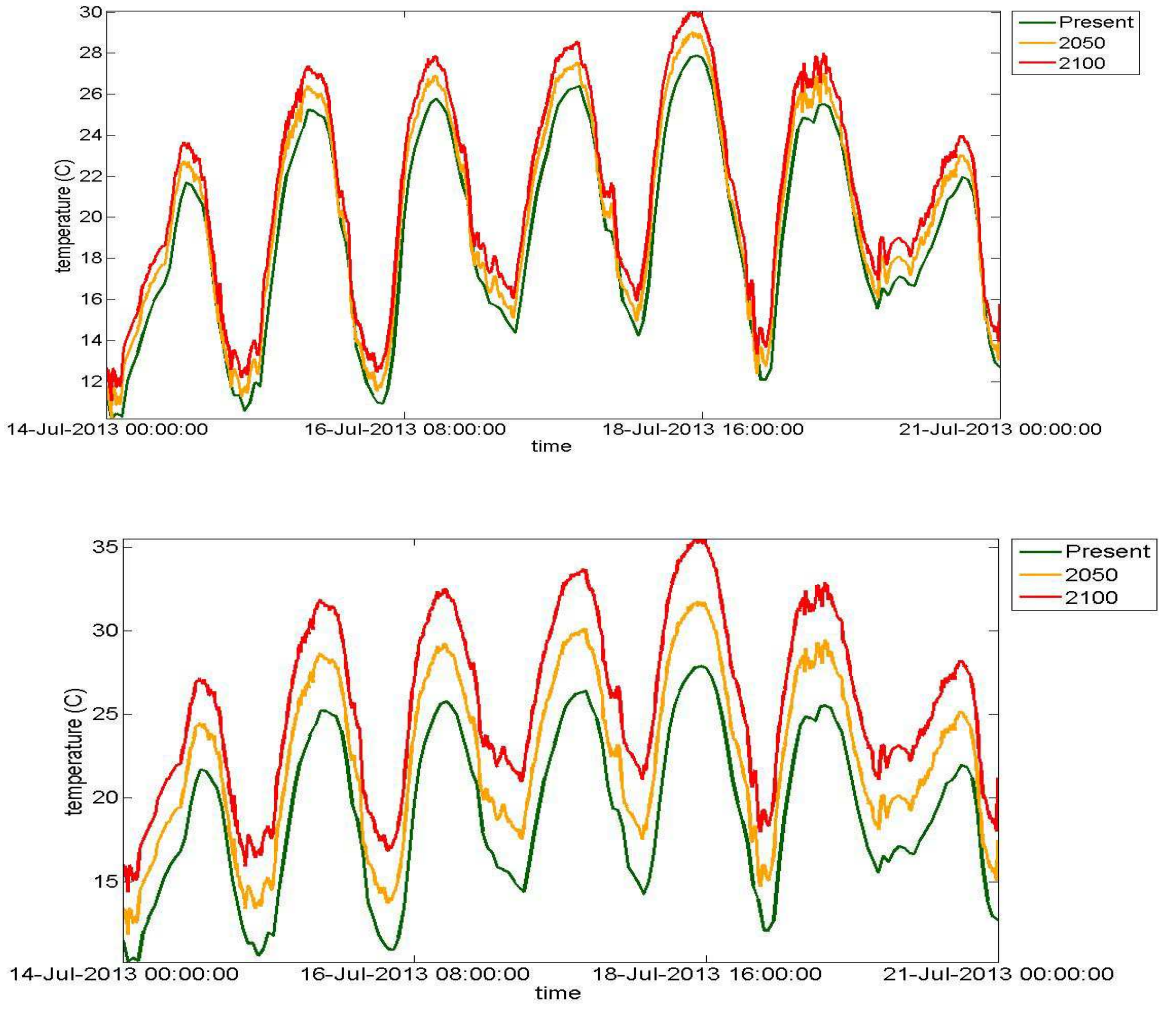

Figure 17, the present rural temperature and the future rural temperature constructed with the climate transformation. The top graph shows the mildest (G) scenario, while the graph in at the bottom resamples the most extreme (W+) scenario. The transformation is based on the week between 14 and 21 July. The scale on the y-axis differ for both graphs.

3.3.1 Urban temperature

In Eq. 13, the urban temperature is dependent on the rural temperature, wind speed, API, NDVI and radiation. If we assume the obtained regression relation to remain valid in a changing climate, we can implement the found time series of the future rural temperature in this formula and thereby calculating the future urban temperature. The constructed time series correspond with the description of the different climate scenarios, and the statistical model has a good fit with the observations, so the combined use should results in the reasonable estimation of the future urban temperature.

Figure 18 shows a time series of the present and future urban temperature at the Markt. Again the temperature increases 1 °C in 2050, and 2 °C in 2100 which is in line with the climate scenario and the findings in the rural case. The temperature tend to be a bit higher in the urban surroundings.

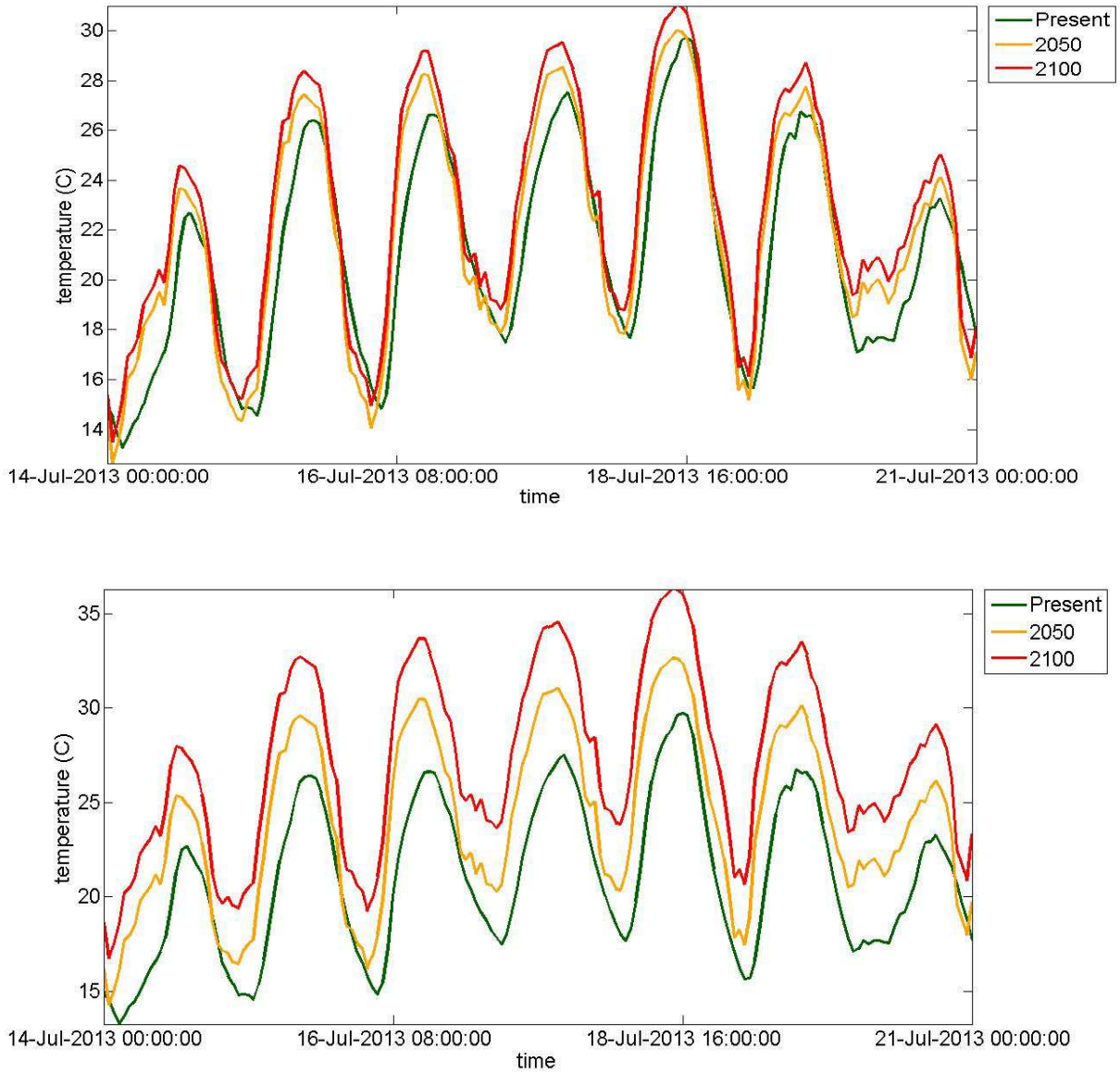

Figure 18, measurements of the present urban temperature at the Markt site for the period 14 July 0:00 UTC until 21 July 0:00 UTC and future urban temperature time series, based on equationEq. **13** and scenario G (top) and scenario W+ (bottom).

For the extreme scenario (W+) a temperature increase of ±3.5 and ±7 °C is forecasted for 2050 and 2100 respectively. This change is slightly less than the change for rural temperature. Probably this has to do with the temperature range. The coefficient for the rural temperature in Eq. 13 is +0.9765, this coefficient is based on temperatures ranging from 2.2 °C to 33.9 °C. The transformed rural temperature is 4 °C higher in 2050 and 8 °C in 2100, thereby outside the range for a considerable time. Temperatures are damped by 0.235% due to the coefficient, higher temperature result in more damping and therefore a possible change in the forecasted urban temperature.

The amount of warm nights (minimum temperature >20 °C) is increasing due to the climate change. The 2013 summer had 5 warm nights, with the mildest scenario (G) this will increase to 8 (12) in 2050 (2100), for the most extreme scenario (W+) this will even increase to 10 (23) in 2050 (2100). Thereby, the changes in (urban) temperature are substantial.

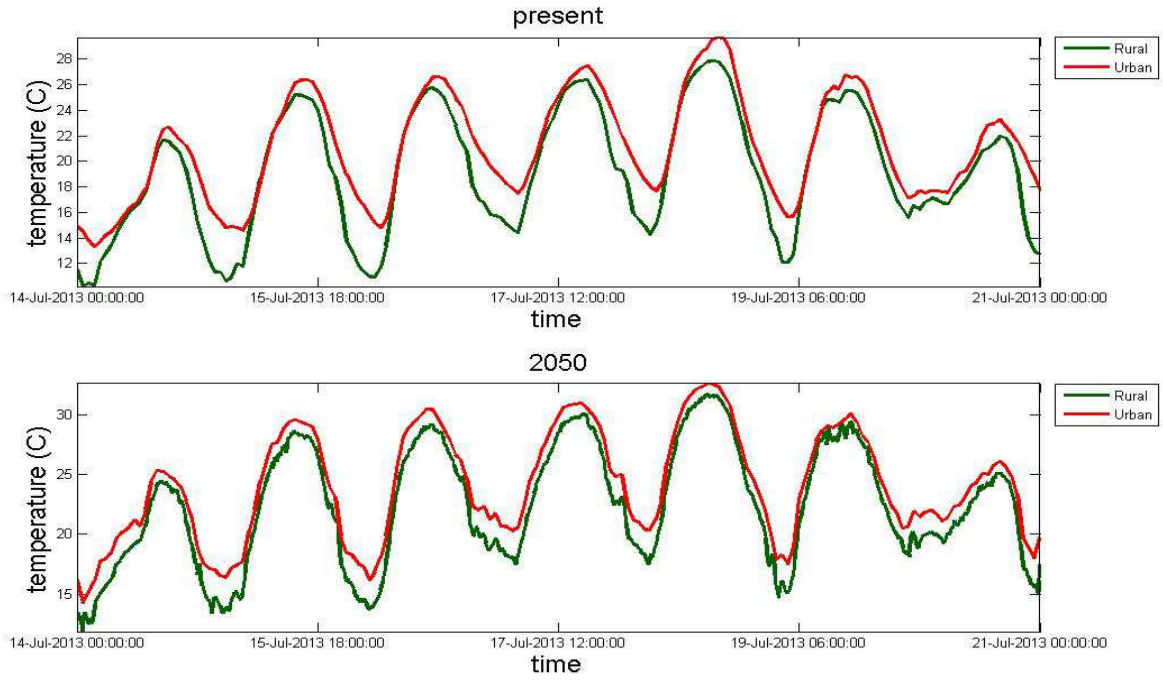

Figure 19, the urban (Markt) and rural temperature as measured in 2013 and constructed for 2050 with the W+ scenario. The y-axis do not have the same scale.

If we would compare the urban and rural temperatures as measured in 2013 and constructed for 2050 (Figure 19) we see that the both graphs look similar. The constructed temperature is fluctuating a little bit more, but the same trends are visible. In both the present and future time series the maximum temperature is approximately 2 ºC warmer at the Markt. The nocturnal temperature differences are slightly smaller in 2050, which might have to do with the coefficient for rural temperature in Eq. 13 as explained above. An increase of the UHI is absent in the preformed transformations and changes in temperature are solely due to changing climate.

4. Conclusions

In this research we have investigated the diurnal and spatial variation of the urban heat island (UHI) in Wageningen by using measurements of 32 stations located in and around Wageningen during the three summer months. We have seen that the UHI is strongest during the night, approximately around 4:00 UTC (which is around sunrise), and has a minimum 3 hours later. The UHI is due to a difference in maximum temperature and a reduced cooling rate in the city. The measurement location Markt (19), which is located in the densely build old town centre, had a typical difference in maximum temperature of 2 °C and a daily maximum UHI of 5 °C during the 2013 summer.

The spatial variation of the urban heat island is large, fluctuations of 2 °C over a distance of a few hundred meters are normal. On average the entire city of Wageningen is warmer than the direct surroundings, the temperature profile has roughly the same shape as the contours of the city. The daily maximum UHI is highest in the southern, oldest part of Wageningen, this can be explained by the high density in this area and the absence of vegetation. A secondary warm spot is located in the a north-western residential area. The reason for this warm spot is not known.

A statistical model is built, using multiple linear regression, with the purpose of forecasting the UHI in Wageningen. We tried to do this for the daily maximum UHI, the difference in minimum temperature and the hourly urban temperature. For all three models we have tested different combinations of 1 to 5 independent variables that were time dependent, location dependent or both. The models for the daily maximum UHI and the difference in minimum temperature didn't had satisfying results, the explained variance and the index of agreement were low, the RMSE was high, and a large part of the errors were systematic.

The model for the hourly urban temperature did had satisfying results. A combination of variables consisting the rural temperature, the logarithm of the wind speed, the Normalized Difference Vegetation Index (NDVI), the Antecedent Precipitation Index (API) and a constructed sum of the incoming shortwave radiation within the city (Rad_{urban}) resulted in a model (Eq. 15) with high explained variance, high index of agreement and low RMSE, with most of the error being unsystematic.

Eq. 15

$$T_{urban} = 0.9765 * T_{rural} - 0.8204 * log(U) - 0.02312 * API - 2.365 * NDVI + 2.392e-08 * Rad_{urban} + 2.706$$

For the final part of this research we have constructed a time series representing the urban temperature in a future climate. Therefore a climate transformation tool has been applied on the rural temperature, and this future rural temperature time series is been used in combination with Eq. 15. The 2050 urban temperatures were 1 to 3.5 ºC higher, depending on the chosen scenario, the 2100 urban temperatures were 2 to 7 ºC higher. These changes were slightly lower than the found results for the rural temperature, This has probably to do with the first coefficient in equationEq. 15, which damps the urban temperature especially with high rural temperatures.

Because the change in rural temperature is larger than the change in urban temperature the urban heat island will decrease in time, according to this simulation. Also the change in urban temperature is solely due to climate change.

5. Discussion

All measurement station were attached to lampposts: agreements were made with the municipality that equipment should be attached in the direction of the street, to avoid collisions with passing vehicles, and shouldn't hang above private property. This limited the possible lampposts to be used, and for some stations we had to deviate from the planned location, for instance location 14 was originally planned in a parallel street and location 15 was attached at the end of the street instead of the planned middle of a street (+- 50 m away). Nevertheless, the locations are evenly spread over the city and the attachment of measurement stations to lampposts gave us the possibility to minimize the disturbance of the sites.

An additional limitation is the attachment at a height of 3 meter (done to prevent vandalism), it deviates from all standards set by the WMO (WMO, 2008), further the relationship between 3 meter temperature and 1.5 meter temperature might be more complicated than the standard lapse rate used in this report. The vertical wind profile (Figure 20) and the consequent vertical temperature profile are strongly dependent on the variation in object height and horizontal distance to objects (Oke, 2004). Both differ greatly between the measurement locations used, resulting in difference in vertical temperature profile.

The measurement stations are equipped with fans which operated at solar power and are therefore only operational with enough solar radiation. Radiation is also the main disturber, and the main reason to have ventilation, therefore no large errors are expected due to the missing of night-time ventilation, but the response time of the temperature sensors might increase at night.

The spatial differences are measured with a high density measurement network, although the distances between station is still somewhere between 300 and 800 meter. From literature it might be expected that within these distances there might be significant differences in temperature, on the scale of tens of meters (Shashua-Bar and Hoffman, 2000, Oliveira et al., 2011) or even on the scale of centimetres (Nichol, 1996). The temperatures might differ for shaded and non-shaded areas (Shashua-Bar and Hoffman, 2000). Due to the close proximity to objects, the stations used in Wageningen can be effected by shade of objects, depending on time of the day and season. Within this

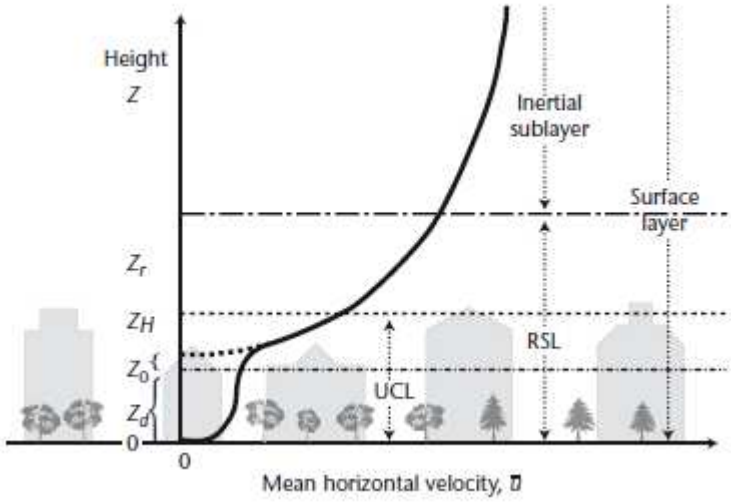

Figure 20, Generalized mean (spatial and temporal) wind velocity (u) profile in a densely developed urban are including the location of the surface layer. The measurement on the height scale are the mean height of the roughness elements (Z_H) the roughness sublayer or blending height (Z_r), the roughness length (Z_0) and zero-plane displacement length (Z_d). The Urban Canopy Layer (UCL) and Roughness sublayer (RSL) are displayed. The dased line represents the profile extrapolated from the Inertial sublayer, the solid line represents the actual profile (Oke, 2004).

thesis report we assumed linear gradient of temperatures between stations and not we have taken into account micrometeorological differences.

The temporal variation of the urban heat island are roughly in line with findings in other cities (Rotach et al., 2005, Johnson, 1985): a maximum UHI at the end of night and the low or even negative UHI during daytime. While in many urban heat island research there are limited measurement sites and focusses are primarily on extreme cases, our goal was to examine the temporal and spatial variation of the UHI in Wageningen. We have seen that there are large differences, both in time and space, in the urban heat island.

the linear regression is only valid within the range of the original data (Table 3,5 and 6). This range is relatively small because of the limited period we have used for this research. Considering the 2013 summer to be relatively warm, dry and sunny (KNMI, 2013) other summers might not be within the range and comparison might be difficult.

In producing the climate transformation multiple assumptions were made. The transformation is based on data from the Haarweg in the period 1976-2005 but applied on the summer data measured at the Veenkampen in the 2013 summer. The two measurement location are only a few km apart and have similar measurement design, as a results, it can be assumed that the change in location has a limited effect. The effects of the transition in reference time might be larger but are not taken into account. The change in temperature from the 1990 climate to the 2013 summer due to climate change is not taken into account, and as already mentioned the 2013 was not an average summer. Due to the design of the transformation tool the change in temperature might be slightly overestimated (the change factor increase with the anomaly), but the found changes are in line with the climate scenarios of the KNMI (Van den Hurk et al., 2006).

An additional assumption is that only the temperature will change due to climate change. Climate change might also effect precipitation, soil moisture, vegetation fractions, NDVI, cloud cover and radiation terms. In this research we have assumed this variables to be non-changing.

Appendix I – References

ARNFIELD, A. J. 2003. Two decades of urban climate research: a review of turbulence, exchanges of energy and water, and the urban heat island. *International journal of climatology,* 23, 1-26.

BAKKER, A. & BESSEMBINDER, J. 2012. Time series transformation tool: description of the program to generate time series consistent with the KNMI'06 climate scenarios. KNMI Technical Report TR-326, De Bilt, The Netherlands. Available from: www. knmi. nl/knmi-library/knmipub_en. html.

BLANCHARD, B. J., MCFARLAND, M. J., SCHMUGGE, T. J. & RHOADES, E. 1981. ESTIMATION OF SOIL MOISTURE WITH API ALGORITHMS AND MICROWAVE EMISSION1. Wiley Online Library.

BOHNENSTENGEL, S., HAMILTON, I., DAVIES, M. & BELCHER, S. 2013. Impact of anthropogenic heat emissions on London's temperatures. *Quarterly Journal of the Royal Meteorological Society*.

BOWLER, D. E., BUYUNG-ALI, L., KNIGHT, T. M. & PULLIN, A. S. 2010. Urban greening to cool towns and cities: A systematic review of the empirical evidence. *Landscape and urban planning,* 97, 147-155.

CHRISTEN, A. & VOGT, R. 2004. Energy and radiation balance of a central European city. *International journal of climatology,* 24, 1395-1421.

CONRADS, L. A. 1975. *Observations of Meteorological Urban Effects: The Heat Island of Utercht.* Rijksuniversiteit te Utrecht.

DOLL, D., CHING, J. & KANESHIRO, J. 1985. Parameterization of subsurface heating for soil and concrete using net radiation data. *Boundary-Layer Meteorology,* 32, 351-372.

FAST, J. D., TORCOLINI, J. C. & REDMAN, R. 2005. Pseudovertical temperature profiles and the urban heat island measured by a temperature datalogger network in Phoenix, Arizona. *Journal of Applied Meteorology,* 44.

FEDORA, M. & BESCHTA, R. 1989. Storm runoff simulation using an antecedent precipitation index (< i> API</i>) model. *Journal of hydrology,* 112, 121-133.

FLOOR, C. 1970. Onderzoek Utrechts stadsklimaat met weerbus. *Hemel Dampkring,* 68, 107-111.

HARMAN, I. N., BEST, M. J. & BELCHER, S. E. 2004. Radiative exchange in an urban street canyon. *Boundary-Layer Meteorology,* 110, 301-316.

HATHWAY, E. & SHARPLES, S. 2012. The interaction of rivers and urban form in mitigating the Urban Heat Island effect: A UK case study. *Building and Environment,* 58, 14-22.

HEUSINKVELD, B. G., VAN HOVE, L. & JACOBS, C. 2012. Ruimtelijke analyse van het stadsklimaat in Arnhem. . Wageningen: Wageningen University.

HEUSINKVELD, B. G., VAN HOVE, L., JACOBS, C., STEENEVELD, G., ELBERS, J., MOORS, E. & HOLTSLAG, A. Use of a mobile platform for assessing urban heat stress in Rotterdam. Proceedings of the 7th Conference on Biometeorology Albert-Ludwigs-University of Freiburg, Germany, 2010. 14.

HOLMER, B., POSTGÅRD, U. & ERIKSSON, M. 2001. Sky view factors in forest canopies calculated with IDRISI. *Theoretical and Applied Climatology,* 68, 33-40.

HUETE, A., DIDAN, K., MIURA, T., RODRIGUEZ, E. P., GAO, X. & FERREIRA, L. G. 2002. Overview of the radiometric and biophysical performance of the MODIS vegetation indices. *Remote Sensing of Environment,* 83, 195-213.

ICHINOSE, T., SHIMODOZONO, K. & HANAKI, K. 1999. Impact of anthropogenic heat on urban climate in Tokyo. *Atmospheric Environment,* 33, 3897-3909.

JACKSON, T. J. 1993. III. Measuring surface soil moisture using passive microwave remote sensing. *Hydrological processes,* 7, 139-152.

JOHNSON, D. 1985. Urban modification of diurnal temperature cycles in Birmingham, UK. *Journal of climatology,* 5, 221-225.

JOHNSON, G. T. & WATSON, I. D. 1984. The determination of view-factors in urban canyons. *Journal of Climate and Applied Meteorology,* 23, 329-335.

KNMI. 2013. *Zomer was warm, droog en zonnig* [Online]. De Bilt. Available: http://www.knmi.nl/cms/content/115141/zomer_was_warm_droog_en_zonnig [Accessed 04-12 2014].

MARCIOTTO, E. R., OLIVEIRA, A. P. & HANNA, S. R. 2010. Modeling study of the aspect ratio influence on urban canopy energy fluxes with a modified wall-canyon energy budget scheme. *Building and Environment,* 45, 2497-2505.

MATZARAKIS, A., RUTZ, F. & MAYER, H. 2010. Modelling radiation fluxes in simple and complex environments: basics of the RayMan model. *International journal of biometeorology,* 54, 131-139.

MEMON, R. A., LEUNG, D. Y. & LIU, C.-H. 2010. Effects of building aspect ratio and wind speed on air temperatures in urban-like street canyons. *Building and Environment,* 45, 176-188.

MERKIN, R. 2004. *The Urban Heat Island's Effect on the diurnal temperature range.* Massachusetts Institute of Technology.

MORRIS, C., SIMMONDS, I. & PLUMMER, N. 2001. Quantification of the influences of wind and cloud on the nocturnal urban heat island of a large city. *Journal of Applied Meteorology,* 40, 169-182.

MYRUP, L. O. 1969. A numerical model of the urban heat island. *Journal of Applied Meteorology,* 8, 908-918.

NICHOL, J. E. 1996. High-resolution surface temperature patterns related to urban morphology in a tropical city: a satellite-based study. *Journal of Applied Meteorology,* 35, 135-146.
OKE, T. R. 1973. City size and the urban heat island. *Atmospheric Environment (1967),* 7, 769-779.
OKE, T. R. 1982. The energetic basis of the urban heat island (Symons Memorial Lecture, 20 May 1980). *Quarterly Journal, Royal Meteorological Society,* 108, 1-24.
OKE, T. R. 2004. *Initial guidance to obtain representative meteorological observations at urban sites*, World Meteorological Organization Geneva.
OLESON, K. W., BONAN, G. & FEDDEMA, J. 2010. Effects of white roofs on urban temperature in a global climate model. *Geophysical Research Letters,* 37.
OLIVEIRA, S., ANDRADE, H. & VAZ, T. 2011. The cooling effect of green spaces as a contribution to the mitigation of urban heat: A case study in Lisbon. *Building and Environment,* 46, 2186-2194.
PARRY, M. L. 2007. *Climate Change 2007: impacts, adaptation and vulnerability: contribution of Working Group II to the fourth assessment report of the Intergovernmental Panel on Climate Change*, Cambridge University Press.
PEEL, M. C., FINLAYSON, B. L. & MCMAHON, T. A. 2007. Updated world map of the Köppen-Geiger climate classification. *Hydrology & Earth System Sciences Discussions,* 4.
RIZWAN, A. M., DENNIS, L. Y. & LIU, C. 2008. A review on the generation, determination and mitigation of Urban Heat Island. *Journal of Environmental Sciences,* 20, 120-128.
ROBITU, M., MUSY, M., INARD, C. & GROLEAU, D. 2006. Modeling the influence of vegetation and water pond on urban microclimate. *Solar Energy,* 80, 435-447.
ROODENBURG, J. 1983. Adaptation of rural minimum temperature forecasts to an urban environment. *Archives for meteorology, geophysics, and bioclimatology, Series B,* 32, 395-401.
ROTACH, M., VOGT, R., BERNHOFER, C., BATCHVAROVA, E., CHRISTEN, A., CLAPPIER, A., FEDDERSEN, B., GRYNING, S.-E., MARTUCCI, G. & MAYER, H. 2005. BUBBLE–an urban boundary layer meteorology project. *Theoretical and Applied Climatology,* 81, 231-261.
SANTAMOURIS, M. 2012. Cooling the cities–a review of reflective and green roof mitigation technologies to fight heat island and improve comfort in urban environments. *Solar Energy*.
SHASHUA-BAR, L. & HOFFMAN, M. 2000. Vegetation as a climatic component in the design of an urban street: An empirical model for predicting the cooling effect of urban green areas with trees. *Energy and buildings,* 31, 221-235.
SILVA, H. R., PHELAN, P. E. & GOLDEN, J. S. 2010. Modeling effects of urban heat island mitigation strategies on heat-related morbidity: a case study for Phoenix, Arizona, USA. *International journal of biometeorology,* 54, 13-22.
SPRONKEN-SMITH, R. & OKE, T. 1999. Scale modelling of nocturnal cooling in urban parks. *Boundary-Layer Meteorology,* 93, 287-312.
STARKE, P., GÖBEL, P. & COLDEWEY, W. 2010. Urban evaporation rates for water-permeable pavements. *Water Science & Technology,* 62.
STEENEVELD, G., KOOPMANS, S., HEUSINKVELD, B. & THEEUWES, N. 2014. Refreshing the role of open water surfaces on mitigating the maximum urban heat island effect. *Landscape and urban planning,* 121, 92-96.
STEENEVELD, G., KOOPMANS, S., HEUSINKVELD, B., VAN HOVE, L. & HOLTSLAG, A. 2011. Quantifying urban heat island effects and human comfort for cities of variable size and urban morphology in the Netherlands. *Journal of Geophysical Research: Atmospheres (1984–2012),* 116.
STEWART, I. D. 2000. Influence of meteorological conditions on the intensity and form of the urban heat island effect in Regina. *The Canadian Geographer/Le Géographe canadien,* 44, 271-285.
STEWART, I. D. 2011. A systematic review and scientific critique of methodology in modern urban heat island literature. *International journal of climatology,* 31, 200-217.
STEWART, I. D. & OKE, T. R. 2012. Local climate zones for urban temperature studies. *Bulletin of the American Meteorological Society,* 93, 1879-1900.
STREILING, S. & MATZARAKIS, A. 2003. Influence of single and small clusters of trees on the bioclimate of a city: a case study. *Journal of Arboriculture,* 29, 309-316.
SVENSSON, M. K. 2004. Sky view factor analysis–implications for urban air temperature differences. *Meteorological Applications,* 11, 201-211.
TAHA, H. 1997. Urban climates and heat islands: albedo, evapotranspiration, and anthropogenic heat. *Energy and buildings,* 25, 99-103.
THEEUWES, N., SOLCEROVÁ, A. & STEENEVELD, G. 2013. Modeling the influence of open water surfaces on the summertime temperature and thermal comfort in the city. *Journal of Geophysical Research: Atmospheres,* 118, 8881-8896.
TOMLINSON, C., PRIETO - LOPEZ, T., BASSETT, R., CHAPMAN, L., CAI, X. M., THORNES, J. & BAKER, C. 2013. Showcasing urban heat island work in Birmingham–measuring, monitoring, modelling and more. *Weather,* 68, 44-49.
TSANGRASSOULIS, A. & SANTAMOURIS, M. 2003. Numerical estimation of street canyon albedo consisting of vertical coated glazed facades. *Energy and buildings,* 35, 527-531.
UN 2011. World Urban prospect: the 2011 revision. New York: United Nation.
UNGER, J. (2004). "Intra-urban relationship between surface geometry and urban heat island: review and new approach." Climate research 27: 253-264.

VAN DEN HURK, B., KLEIN TANK, A., LENDERINK, G., VAN ULDEN, A., VAN OLDENBORGH, G., KATSMAN, C., VAN DEN BRINK, H., KELLER, F., BESSEMBINDER, J. & BURGERS, G. 2006. ***KNMI climate change scenarios 2006 for the Netherlands*****, KNMI De Bilt.**

WATKINS, R., PALMER, J., KOLOKOTRONI, M. & LITTLEFAIR, P. 2002. The London Heat Island: results from summertime monitoring. ***Building Services Engineering Research and Technology,*** **23, 97-106.**

WEERSTATISTIEK. 2014. ***Weather Statistics*** **[Online]. Available: http://www.weerstatstiek.nl [Accessed 04-12 2014].**

WMO 2008. ***Guide to meterological instruments and methods of observation*****, Secretariat of the World Meteorological Organization.**

XIAO, R.-B., OUYANG, Z.-Y., ZHENG, H., LI, W.-F., SCHIENKE, E. W. & WANG, X.-K. 2007. Spatial pattern of impervious surfaces and their impacts on land surface temperature in Beijing, China. ***Journal of Environmental Sciences,*** **19, 250-256.**

Appendix II – specifications measurement equipment

Specifications Data logger	
Input Ports:	5 channels, each supporting 12-bit analog, 32-bit digital, or pulse, compatible with any Decagon Devices sensor
Port Type:	3.5 mm "stereo jack" connector
Data Storage:	1 MB (36,000 scans of all 5 ports)
Memory Type:	Non-Volatile Flash
Logging Interval:	5 minutes to 24 hours, logged data is 1-minute average of user-specified interval
Data Transmission Frequency:	Up to six times/day.
Operating Environment:	-30° - 60°C, up to 100% RH
Battery Capacity:	5 AA alkaline or lithium batteries
Battery service life:	6+ months
External power needs:	None needed
Enclosure:	Weatherproof, impact and UV-resistant polymer
Enclosure Dimensions:	12.7 cm x 20.3 cm x 5.1 cm (5 in x 8 in x 2 in)
Enclosure rating:	IP55, NEMA 3R
Enclosure access:	Hinged door with eyelet for securing with user-supplied padlock
Mounting:	3.8 cm (1.5 inch) mast or wall mount
Local Communication:	Dedicated serial port 3.5 mm stereo jack for use with the Decagon Serial Cable Adapter (SCA) or Decagon USB Cable Adaptor (UCA)
Cellular Frequencies:	Quad-band (850/900/1800/1900 MHz) GSM/GPRS for use worldwide.

Specifications VP-3 Temperature/humidity sensor	
Humidity Resolution	0.1% RH
Temperature Resolution	0.1°C
Vapor Pressure Resolution	0.01 kPa
Humidity Range	0-100% RH
Temperature Range	-40°C to 80°C
Vapor Pressure Range	0-47 kPa
Sensor Type	Digital Capacitance and Thermistor
Output	RS232, SDI-12
Operating Environment	-40°C to 80°C
Cable Length	5 m
Cable Connector Types	3.5 mm "stereo" plug or three-wire
Power Requirements	3.6-15 VDC, 0.03 mA quiescent, 4 mA during 300 ms measurement
Sensor Dimensions	5.4 cm x 1.96 cm

Humidity Accuracy [%RH]

Humidity [%RH]	0°C	10°C	20°C	30°C	40°C	50°C	60°C	70°C	80°C
100%	±5%	±5%	±5%	±5%	±5%	±5%	±5%	±6%	±10%
95%	±5%	±5%	±4%	±4%	±4%	±4%	±4%	±5%	±8%
90%	±5%	±4%	±2%	±2%	±3%	±3%	±4%	±5%	±8%
85%	±5%	±4%	±2%	±2%	±3%	±3%	±4%	±5%	±8%
80%	±4%	±4%	±2%	±2%	±3%	±3%	±3%	±4%	±6%
75%	±4%	±4%	±2%	±2%	±3%	±3%	±3%	±4%	±6%
70%	±4%	±4%	±2%	±2%	±3%	±3%	±3%	±4%	±6%
65%	±4%	±4%	±2%	±2%	±3%	±3%	±3%	±4%	±6%
60%	±4%	±3%	±2%	±2%	±2%	±2%	±2%	±3%	±5%
55%	±4%	±2%	±2%	±2%	±2%	±2%	±2%	±3%	±5%
50%	±4%	±2%	±2%	±2%	±2%	±2%	±2%	±3%	±5%
45%	±4%	±2%	±2%	±2%	±2%	±2%	±2%	±3%	±4%
40%	±4%	±2%	±2%	±2%	±2%	±2%	±2%	±3%	±4%
35%	±4%	±3%	±2%	±2%	±2%	±2%	±2%	±3%	±4%
30%	±4%	±3%	±2%	±2%	±2%	±2%	±2%	±3%	±4%
25%	±4%	±3%	±2%	±2%	±2%	±2%	±2%	±3%	±4%
20%	±4%	±4%	±2%	±2%	±3%	±3%	±3%	±3%	±4%
15%	±5%	±4%	±2%	±2%	±3%	±3%	±4%	±4%	±5%
10%	±8%	±5%	±3%	±3%	±4%	±4%	±4%	±5%	±8%
5%	±8%	±8%	±5%	±5%	±5%	±5%	±5%	±6%	±10%
0%	±12%	±12%	±5%	±5%	±6%	±6%	±6%	±10%	±12%

Temperature [°C]

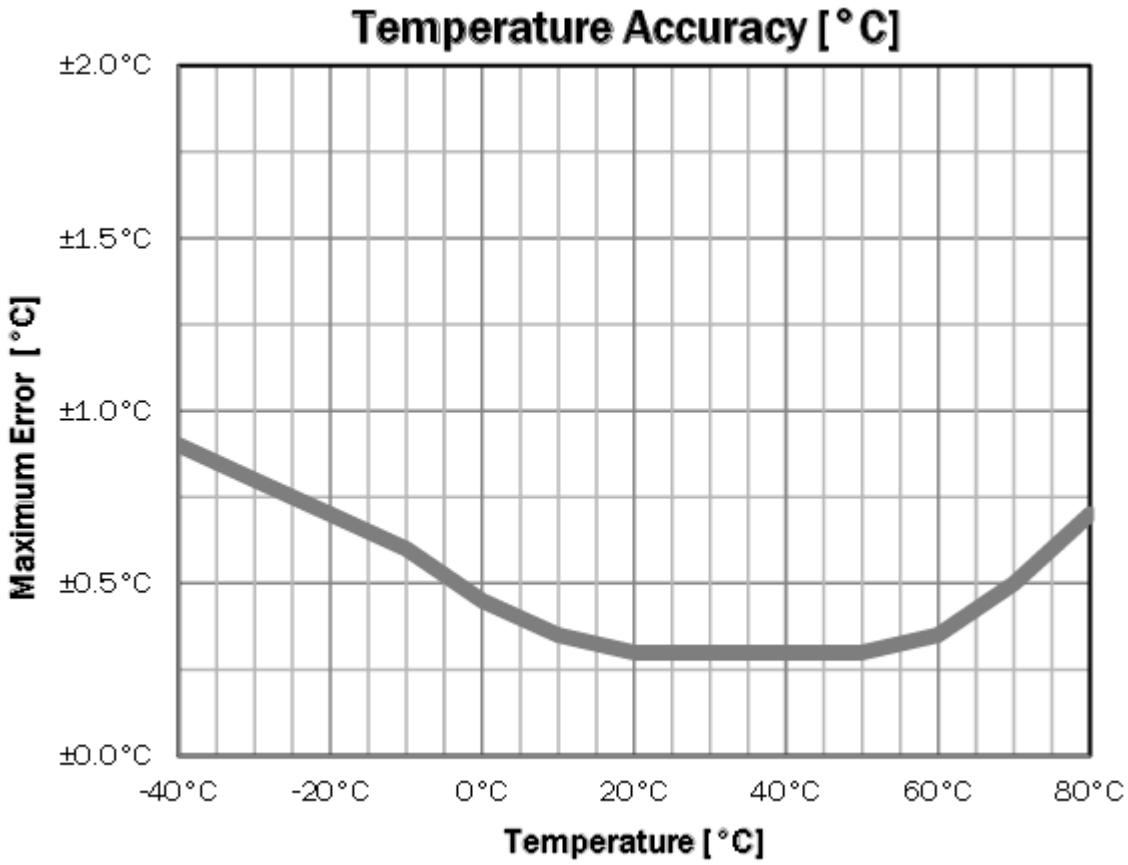
Temperature Accuracy [°C]
±2.0°C
±1.5°C
±1.0°C
±0.5°C
±0.0°C
Maximum Error [°C]
-40°C
-20°C
0°C
20°C
40°C
60°C
80°C
Temperature [°C]

Radiation Shield	
Radiation Shield Dimensions	197 mm height, 184 mm diameter
Radiation Shield Weight	1.6 kg
Fan Aspiration Rate	0.9 m/s At insolation rate of 1040 W/m^2
Radiation-Induced Temperature Error	0.33°C At insolation rate of 1040 W/m^2
Operating Temperature	-20 to +55°C
Housing Material	UV-resistant plastic

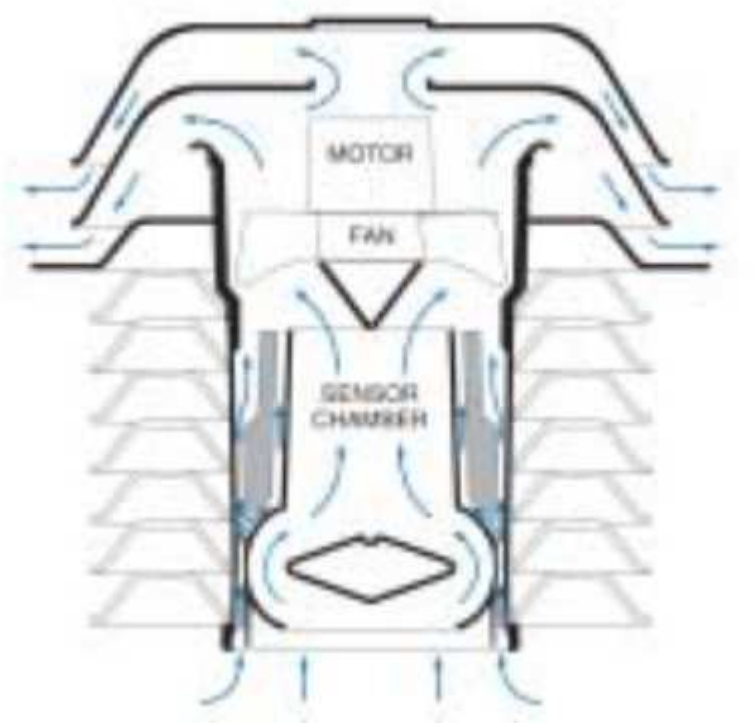

Solar Panel	
Operating Temperature	-40 to +65°C
Housing Material	Rugged ASA Plastic
Solar Panel	
Nominal power	5 watt
Voc	21.6V
Isc	300mA
Vmp	18V
Imp	277mA

Appendix III - Validation of statistical model

For evaluate the results of the multiple linear regression a number of indicators will be used. $\overline{O}$ is the average of the observed data. $\overline{P}$ is the average of the predicted value. s_o is the standard deviation of the observed values. s_p is the standard deviation of the predicted value. N is the amount of observations used for regression. MAE is the Mean Absloute Error.

Eq. 16

$$MAE = N^{-1} \sum_{i=1}^{N} |P_i - O_i|$$

$RMSE$ is the root mean square error, where $RMSE_s$ is the root of the systematic part of the mean square error.

Eq. 17

$$RMSE_s = \left[N^{-1} \sum_{i=1}^{N} \left(\hat{P}_i - O_i \right)^2 \right]^{0.5}$$

Eq. 18

$$\hat{P}_i = a + bO_i$$

Where a and b are estimated using a least squares regression between O and P. $RMSE_u$ is the root of the unsystematic part of the mean square error. MSE = MSE_s + MSE_u

Eq. 19

$$RMSE_u = \left[N^{-1} \sum_{i=1}^{N} \left(O_i - \hat{P}_i \right)^2 \right]^{0.5}$$

d is the index of agreement between the predicted and the observed data. It is a measure of the degree to which a model's predictions are error free. It varies between 0 and 1, in which 0 is a complete disagreement and 1 is a perfect agreement.

Eq. 20

$$d = 1 - \frac{\sum_{i=1}^{N} (P_i - O_i)^2}{\sum_{i=1}^{N} \left(|P_i`| + |O_i`| \right)^2}$$

In which $P_i` = P_i - \overline{O}_i$ and $O_i` = O_i - \overline{O}_i$.

R^2 is adjusted for the number of coefficients.

Appendix IV – Climate transformation

The 90th, 50th and 10th temperature percentiles are determined from the observations ("current climate") and are denoted (T^c_{90}, T^c_{50} and T^c_{10}) respectively. The future percentiles (T^f_{90}, T^f_{50} and T^f_{10}) are calculated by adding the change factors (ΔT_{90}, ΔT_{50} and ΔT_{10}, Eq. 21) that belong to the selected scenario and time horizon. This is applied for each calendar month separately. The change factors are determined by the KNMI and can be found in Appendix V.

Eq. 21

$$\begin{aligned} T^f_{90} &= T^c_{90} + \Delta T_{90} \\ T^f_{50} &= T^c_{50} + \Delta T_{50} \\ T^f_{10} &= T^c_{10} + \Delta T_{10} \end{aligned}$$

Each value of the temperature in the transformed temperature time series, T^f ("future climate") is derived from the reference time series T^c using a scaling relation that is based on the distance of T^c to the median:

Eq. 22

$$T^f = T^f_{50} + \alpha(T^c - T^c_{50})$$

In which T^f is the transformed value of the temperature in the historical time series T^c, and α is a scaling factor that is different for values smaller or higher than the median of the reference time series:

Eq. 23

$$\alpha = \begin{cases} \dfrac{T^f_{90} - T^f_{50}}{T^c_{90} - T^c_{50}} & T^c > T^c_{50} \\ \dfrac{T^f_{10} - T^f_{50}}{T^c_{10} - T^c_{50}} & T^c < T^c_{50} \end{cases}$$

This procedure implies that the changes for values higher than the 90th and lower than the 10th percentile are linearly extrapolated from the changes between the 50th and 90th or the changes between the 50th and 10th percentiles. An example is given for the 99th percentile:

Eq. 24

$$\Delta T_{99} = \Delta T_{50} + \beta(\Delta T_{90} - \Delta T_{50})$$

In which β:

Eq. 25

$$\beta = \frac{T^c_{99} - T^c_{50}}{T^c_{90} - T^c_{50}}$$

In the transformation tool the changes of the 10th, 50th and 90th percentiles are given explicitly for 2050 and 2100, compared to the climate around 1990. For all other percentile the changes are calculated based on equation Eq. 22Eq. 23.

The transition from daily values (on which the transformation tool is based) to hourly values is been done using a conversion factor per day (X).

Eq. 26

$$X = \frac{T^f}{T^c}$$

For every day this conversion factor is used to transform the hourly values of the historical time series to future hourly values.

Eq. 27

$$T^f_{\text{hourly}} = T^c_{hourly} * X$$

Appendix V - Change factors for the temperature transformation tool

Table 8, 10th percentile per calendar month of the average daily temperature change (in degrees Celsius) around 2050 compared to 1976-2005.

month	G	G+	W	W+
1	1	1.41	2.01	2.82
2	1	1.4	2	2.8
3	0.98	1.36	1.96	2.73
4	0.95	1.3	1.9	2.6
5	0.92	1.23	1.84	2.45
6	0.9	1.15	1.8	2.31
7	0.9	1.09	1.79	2.18
8	0.9	1.06	1.8	2.12
9	0.93	1.1	1.84	2.2
10	0.96	1.23	1.91	2.45
11	0.99	1.33	1.97	2.66
12	1	1.39	2	2.78

Table 9, 50th percentile per calendar month of the average daily temperature change (in degrees Celsius) around 2050 compared to 1976-2005.

month	G	G+	W	W+
1	0.9	1.09	1.8	2.29
2	0.9	1.1	1.8	2.3
3	0.9	1.14	1.78	2.36
4	0.9	1.2	1.75	2.47
5	0.9	1.27	1.72	2.59
6	0.9	1.35	1.7	2.71
7	0.9	1.41	1.7	2.82
8	0.9	1.44	1.7	2.87
9	0.9	1.4	1.72	2.8
10	0.9	1.27	1.76	2.59
11	0.9	1.17	1.79	2.42
12	0.9	1.11	1.8	2.32

Table 10, 90th percentile per calendar month of the average daily temperature change (in degrees Celsius) around 2050 compared to 1976-2005.

month	G	G+	W	W+
1	0.79	0.98	1.69	1.85
2	0.8	1	1.71	1.9
3	0.84	1.1	1.75	2.1
4	0.9	1.27	1.85	2.48
5	0.96	1.46	1.94	2.89
6	1	1.66	1.99	3.29
7	1.01	1.83	2.01	3.67
8	1	1.91	1.99	3.84
9	0.96	1.8	1.94	3.6
10	0.89	1.46	1.84	2.89
11	0.83	1.18	1.75	2.29
12	0.8	1.02	1.71	1.95

Appendix VI – relationship between UHI and individual independent variables

The following figures show the relationship between the independent variables of Eq. 13 and Eq. 14 with the urban heat island. For some figures the average data is used instead of hourly data to improve the image.

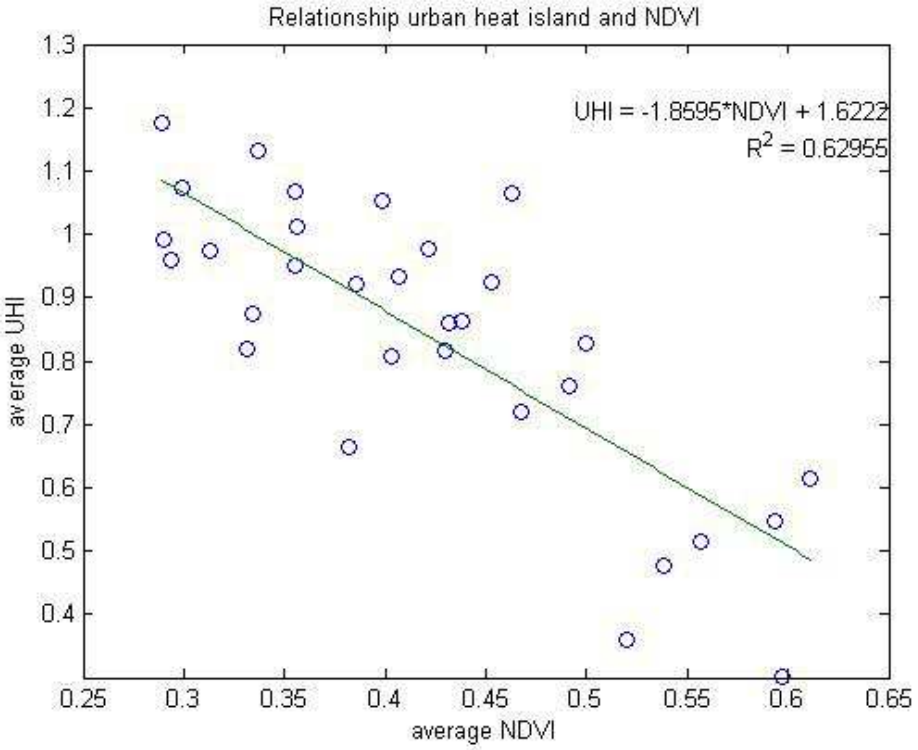

Figure 21, the relationship between the average urban heat island and the average NDVI.

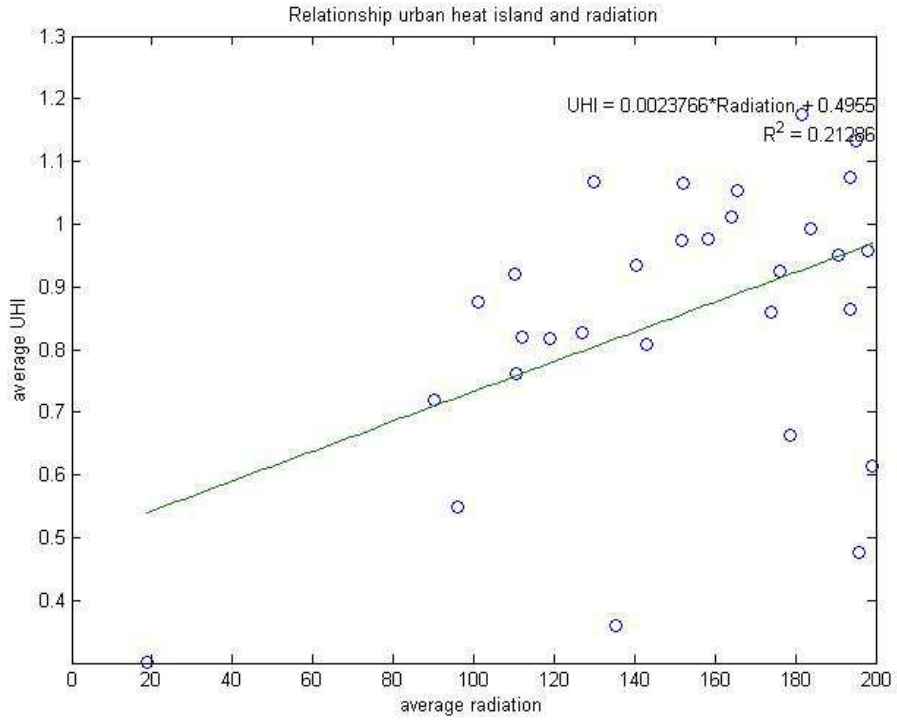

Figure 22, the relationship between the average urban heat island and the constructed average incoming shortwave radiation at the urban locations.

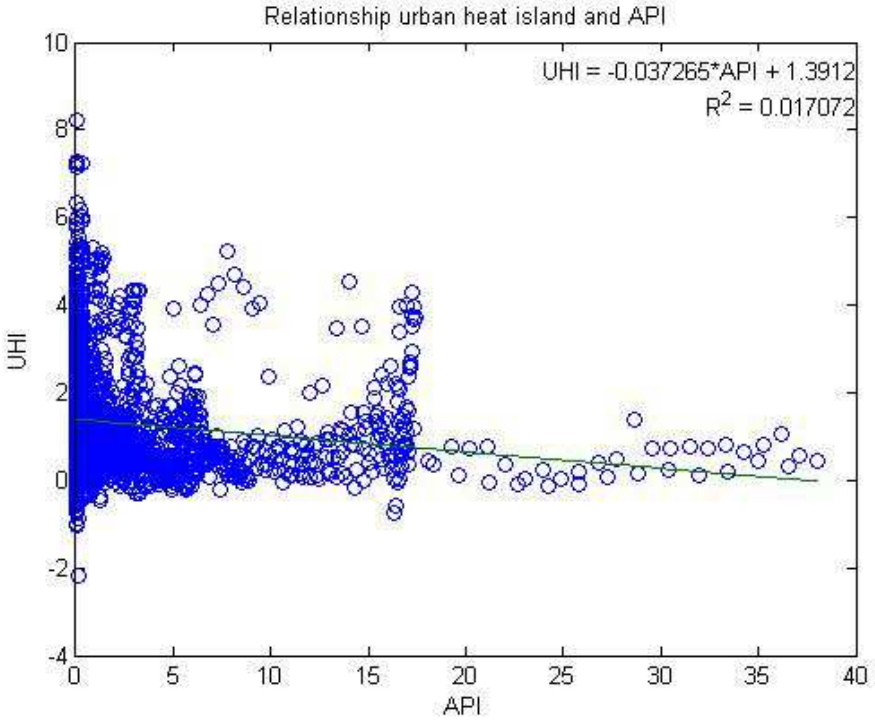

Figure 23, the relationship between the average urban heat island at location Markt and the Antecedent Precipitation Index (API).

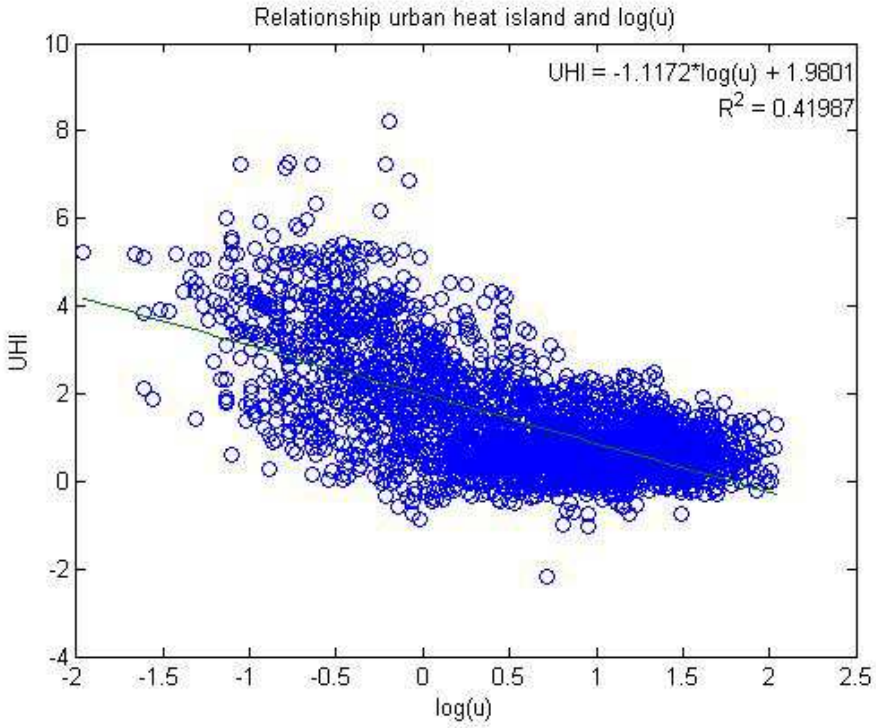

Figure 24, the relationship between the UHI and the logarithm of the wind speed.

location	1	
street	Goudenregenstraat	
latitude	51.971997°	
longitude	5.677241°	
logger	d2225	
local climate zone	6	
Average Summer Temperature	18.615	°C
Minimum Summer Temperature	6.2058	°C
Maximum Summer Temperature	36.747	°C
Average Nighttime Temperature	18.121	°C
Average Daytime Temperature	20.848	°C
Average Summer UHI	1.2882	°C
Average UHI_max	2.7756	°C
Maximum UHI_max	6.1891	°C
Average UHI_diffmin	1.7879	°C
Maximum UHI_diffmin	4.8175	°C

Sky View Photograph

Top-bottom: North, East, South and West.

Average DTR	9.6649	°C
Maximum DTR	16.408	°C
Average NDVI	0.37425	-
Sky View Factor (Holmer et al, 2001)	0.8045	-
built	35	%
impervious	82.5	%
open	55	%
paved	47.5	%
vegetated	25	%
water	0	%

location	2	
street	Ceresstraat	
latitude	51.970020°	
longitude	5.671409°	
logger	d2228	
local climate zone	6	
Average Summer Temperature	18.554	°C
Minimum Summer Temperature	6.4583	°C
Maximum Summer Temperature	35.183	°C
Average Nighttime Temperature	18.134	°C
Average Daytime Temperature	20.492	°C
Average Summer UHI	1.2273	°C
Average UHI_max	3.0542	°C
Maximum UHI_max	7.7483	°C
Average UHI_diffmin	2.0922	°C
Maximum UHI_diffmin	5.6616	°C

Sky View Photograph

Top-bottom: North, East, South and West.

Average DTR	8.5291	°C
Maximum DTR	15.925	°C
Average NDVI	0.32937	-
Sky View Factor (Holmer et al, 2001)	0.73075	-
built	35	%
impervious	82.5	%
open	57.5	%
paved	47.5	%
vegetated	7.5	%
water	0	%

location	3	
street	Van ‘t Hoffstraat	
latitude	51.978244°	
longitude	5.672166°	
logger	d2237	
local climate zone	5	
Average Summer Temperature	18.511	°C
Minimum Summer Temperature	5.9426	°C
Maximum Summer Temperature	35.218	°C
Average Nighttime Temperature	18.124	°C
Average Daytime Temperature	20.636	°C
Average Summer UHI	1.1836	°C
Average UHI_max	2.7441	°C
Maximum UHI_max	5.9343	°C
Average UHI_diffmin	1.889	°C
Maximum UHI_diffmin	5.4209	°C

Sky View Photograph

Top-bottom: North, East, South and West.

Average DTR	8.9251	°C
Maximum DTR	15.508	°C
Average NDVI	0.41315	-
Sky View Factor (Holmer et al, 2001)	0.7206	-
built	35	%
impervious	77.5	%
open	45	%
paved	42.5	%
vegetated	25	%
water	0	%

location	4	
street	Ooststeeg	
latitude	51.977161°	
longitude	5.658090°	
logger	d2245	
local climate zone	6	
Average Summer Temperature	18.401	°C
Minimum Summer Temperature	5.3799	°C
Maximum Summer Temperature	35.647	°C
Average Nighttime Temperature	18.116	°C
Average Daytime Temperature	20.552	°C
Average Summer UHI	1.0743	°C
Average UHI_max	2.5599	°C
Maximum UHI_max	5.8849	°C
Average UHI_diffmin	1.6566	°C
Maximum UHI_diffmin	4.9565	°C

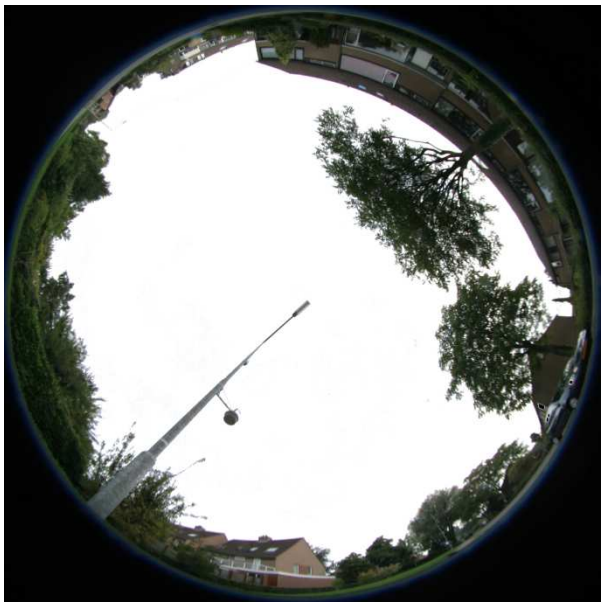

Sky View Photograph

Top-bottom: North, East, South and West.

Average DTR	9.2014	°C
Maximum DTR	16.133	°C
Average NDVI	0.44316	-
Sky View Factor (Holmer et al, 2001)	0.72733	-
built	20	%
impervious	50	%
open	60	%
paved	30	%
vegetated	45	%
water	0	%

location	5	
street	Roghorst	
latitude	51.979936°	
longitude	5.666355°	
logger	d2240	
local climate zone	6	
Average Summer Temperature	18.591	°C
Minimum Summer Temperature	6.6843	°C
Maximum Summer Temperature	35.809	°C
Average Nighttime Temperature	18.127	°C
Average Daytime Temperature	20.814	°C
Average Summer UHI	1.0783	°C
Average UHI_max	2.4673	°C
Maximum UHI_max	5.6409	°C
Average UHI_diffmin	1.6409	°C
Maximum UHI_diffmin	5.3209	°C

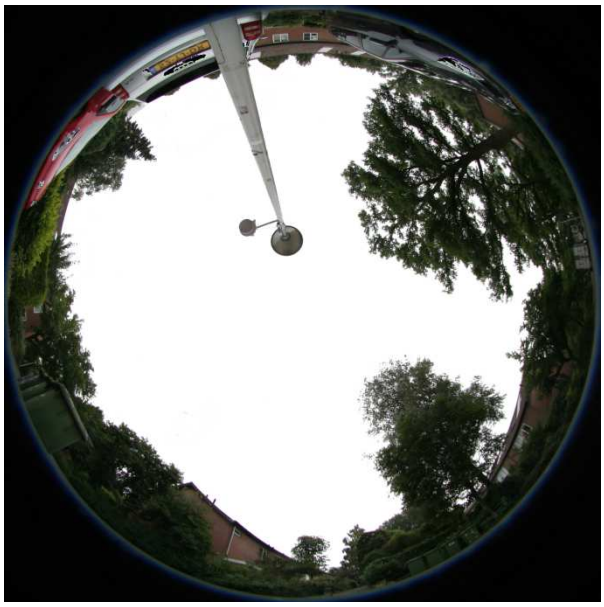

Sky View Photograph

Top-bottom: North, East, South and West.

Average DTR	9.3308	°C
Maximum DTR	16.075	°C
Average NDVI	0.47006	-
Sky View Factor (Holmer et al, 2001)	0.6424	-
built	27.5	%
impervious	77.5	%
open	55	%
paved	50	%
vegetated	32.5	%
water	0	%

location	6	
street	Einthovenstraat	
latitude	51.978622°	
longitude	5.677523°	
logger	d2230	
local climate zone	6	
Average Summer Temperature	18.647	°C
Minimum Summer Temperature	5.6999	°C
Maximum Summer Temperature	36.125	°C
Average Nighttime Temperature	18.118	°C
Average Daytime Temperature	20.979	°C
Average Summer UHI	1.3195	°C
Average UHI_max	2.7014	°C
Maximum UHI_max	6.3416	°C
Average UHI_diffmin	1.6997	°C
Maximum UHI_diffmin	5.2199	°C

Sky View Photograph

Top-bottom: North, East, South and West.

Average DTR	9.5118	°C
Maximum DTR	16.342	°C
Average NDVI	0.39706	-
Sky View Factor (Holmer et al, 2001)	0.747	-
built	27.5	%
impervious	62.5	%
open	35	%
paved	35	%
vegetated	40	%
water	0	%

location	7	
street	Jagerskamp	
latitude	51.975493°	
longitude	5.679528°	
logger	d2234	
local climate zone	6	
Average Summer Temperature	18.371	°C
Minimum Summer Temperature	5.5166	°C
Maximum Summer Temperature	35.967	°C
Average Nighttime Temperature	18.112	°C
Average Daytime Temperature	20.589	°C
Average Summer UHI	1.0441	°C
Average UHI_max	2.5792	°C
Maximum UHI_max	5.1733	°C
Average UHI_diffmin	1.5092	°C
Maximum UHI_diffmin	4.7616	°C

Sky View Photograph

Top-bottom: North, East, South and West.

Average DTR	9.3154	°C
Maximum DTR	15.817	°C
Average NDVI	0.42515	-
Sky View Factor (Holmer et al, 2001)	0.58875	-
built	42.5	%
impervious	75	%
open	37.5	%
paved	32.5	%
vegetated	25	%
water	0	%

location	8	
street	Mondriaanlaan	
latitude	51.981079°	
longitude	5.653066°	
logger	d2235	
local climate zone	6	
Average Summer Temperature	18.565	°C
Minimum Summer Temperature	5.6049	°C
Maximum Summer Temperature	35.722	°C
Average Nighttime Temperature	18.121	°C
Average Daytime Temperature	20.753	°C
Average Summer UHI	1.2379	°C
Average UHI_max	2.728	°C
Maximum UHI_max	6.4615	°C
Average UHI_diffmin	1.797	°C
Maximum UHI_diffmin	4.8065	°C

Sky View Photograph

Top-bottom: North, East, South and West.

Average DTR	9.1366	°C
Maximum DTR	15.983	°C
Average NDVI	0.46487	-
Sky View Factor (Holmer et al, 2001)	0.6478	-
built	42.5	%
impervious	77.5	%
open	35	%
paved	35	%
vegetated	35	%
water	0	%

location	9	
street	Lombardi	
latitude	51.974688°	
longitude	5.657957°	
logger	d2223	
local climate zone	9	
Average Summer Temperature	18.411	°C
Minimum Summer Temperature	5.1534	°C
Maximum Summer Temperature	35.378	°C
Average Nighttime Temperature	18.114	°C
Average Daytime Temperature	20.642	°C
Average Summer UHI	1.0836	°C
Average UHI_max	2.4668	°C
Maximum UHI_max	6.2184	°C
Average UHI_diffmin	1.5541	°C
Maximum UHI_diffmin	4.9651	°C

Sky View Photograph

Top-bottom: North, East, South and West.

Average DTR	9.3703	°C
Maximum DTR	16.292	°C
Average NDVI	0.43668	-
Sky View Factor (Holmer et al, 2001)	0.85275	-
built	25	%
impervious	45	%
open	45	%
paved	20	%
vegetated	60	%
water	0	%

location	10	
street	Boeslaan	
latitude	51.969768°	
longitude	5.686413°	
logger	d2194	
local climate zone	6	
Average Summer Temperature	18.497	°C
Minimum Summer Temperature	6.1415	°C
Maximum Summer Temperature	35.558	°C
Average Nighttime Temperature	18.124	°C
Average Daytime Temperature	20.666	°C
Average Summer UHI	1.17	°C
Average UHI_max	2.7454	°C
Maximum UHI_max	7.6299	°C
Average UHI_diffmin	1.8811	°C
Maximum UHI_diffmin	6.5382	°C

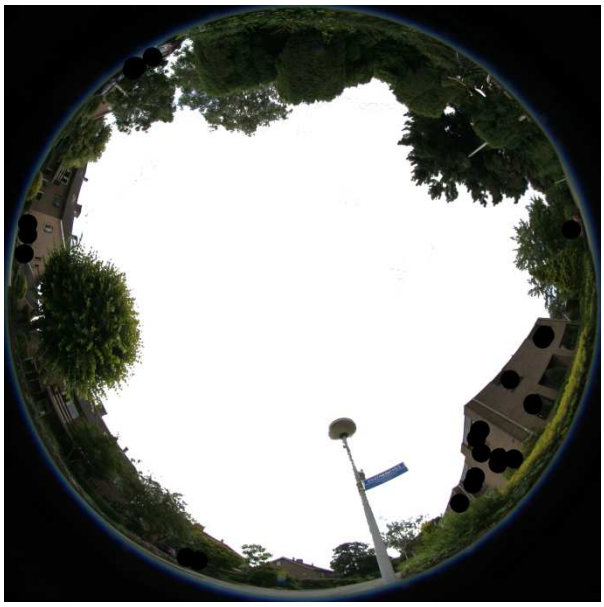

Sky View Photograph

Top-bottom: North, East, South and West.

Average DTR	9.0931	°C
Maximum DTR	16.025	°C
Average NDVI	0.46752	-
Sky View Factor (Holmer et al, 2001)	0.776	-
built	20	%
impervious	60	%
open	45	%
paved	40	%
vegetated	35	%
water	0	%

location	11	
street	Irenestraat	
latitude	51.970957°	
longitude	5.659366°	
logger	d2227	
local climate zone	6	
Average Summer Temperature	18.59	°C
Minimum Summer Temperature	6.4632	°C
Maximum Summer Temperature	35.672	°C
Average Nighttime Temperature	18.13	°C
Average Daytime Temperature	20.632	°C
Average Summer UHI	1.2629	°C
Average UHI_max	2.9477	°C
Maximum UHI_max	6.4699	°C
Average UHI_diffmin	2.0066	°C
Maximum UHI_diffmin	5.5065	°C

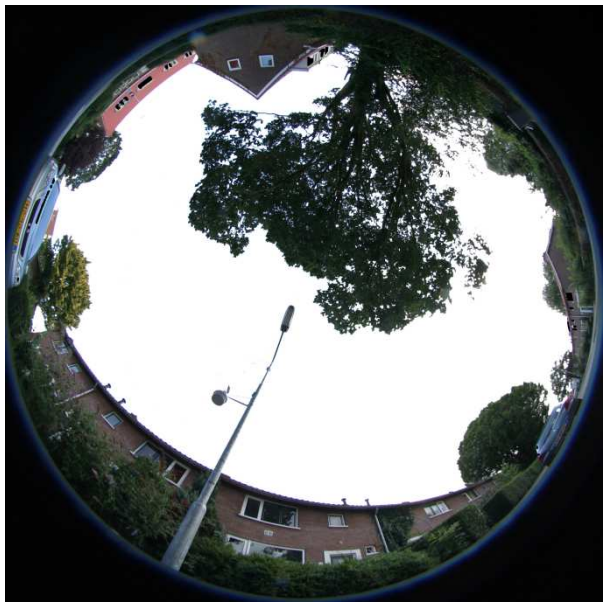

Sky View Photograph

Top-bottom: North, East, South and West.

Average DTR	8.837	°C
Maximum DTR	15.833	°C
Average NDVI	0.31409	-
Sky View Factor (Holmer et al, 2001)	0.63775	-
built	55	%
impervious	75	%
open	25	%
paved	20	%
vegetated	15	%
water	0	%

location	12	
street	Thorbeckestraat	
latitude	51.966323°	
longitude	5.653608°	
logger	d2195	
local climate zone	5	
Average Summer Temperature	18.319	°C
Minimum Summer Temperature	6.3563	°C
Maximum Summer Temperature	34.59	°C
Average Nighttime Temperature	18.126	°C
Average Daytime Temperature	20.197	°C
Average Summer UHI	0.99179	°C
Average UHI_max	2.9258	°C
Maximum UHI_max	6.7647	°C
Average UHI_diffmin	1.9112	°C
Maximum UHI_diffmin	5.3847	°C

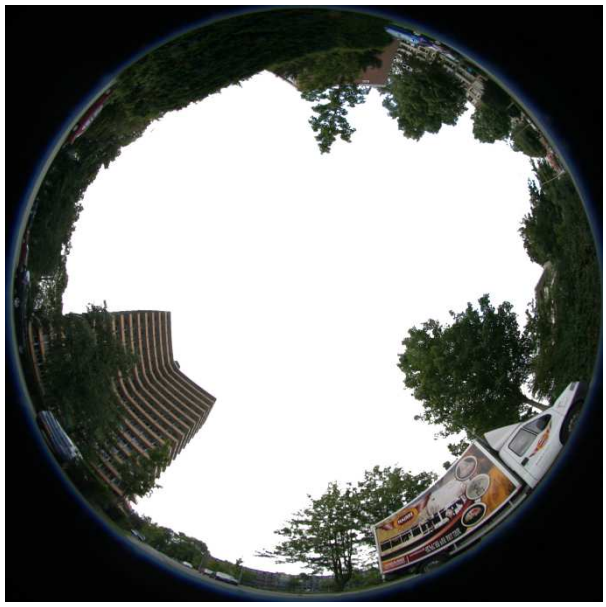

Sky View Photograph

Top-bottom: North, East, South and West.

Average DTR	8.4993	°C
Maximum DTR	15.525	°C
Average NDVI	0.40375	-
Sky View Factor (Holmer et al, 2001)	0.60775	-
built	25	%
impervious	60	%
open	40	%
paved	35	%
vegetated	50	%
water	20	%

location	13	
street	Lijnbaanstraat	
latitude	51.969525°	
longitude	5.663064°	
logger	d2241	
local climate zone	6	
Average Summer Temperature	18.704	°C
Minimum Summer Temperature	6.4132	°C
Maximum Summer Temperature	35.813	°C
Average Nighttime Temperature	18.134	°C
Average Daytime Temperature	20.774	°C
Average Summer UHI	1.377	°C
Average UHI_max	3.0206	°C
Maximum UHI_max	6.9115	°C
Average UHI_diffmin	2.0886	°C
Maximum UHI_diffmin	5.5915	°C

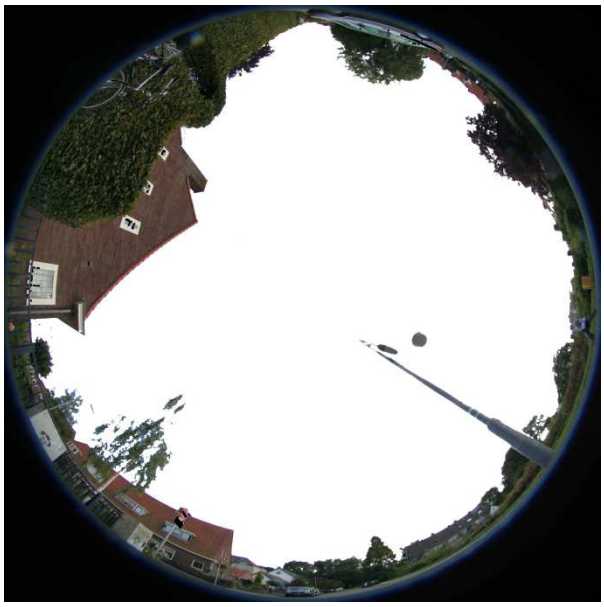

Sky View Photograph

Top-bottom: North, East, South and West.

Average DTR	8.9584	°C
Maximum DTR	15.942	°C
Average NDVI	0.34134	-
Sky View Factor (Holmer et al, 2001)	0.8994	-
built	45	%
impervious	70	%
open	25	%
paved	25	%
vegetated	30	%
water	0	%

location	14	
street	Hinkeloordseweg	
latitude	51.966353°	
longitude	5.674717°	
logger	d2222	
local climate zone	6	
Average Summer Temperature	18.678	°C
Minimum Summer Temperature	6.1617	°C
Maximum Summer Temperature	35.912	°C
Average Nighttime Temperature	18.126	°C
Average Daytime Temperature	20.937	°C
Average Summer UHI	1.3514	°C
Average UHI_max	2.8242	°C
Maximum UHI_max	8.185	°C
Average UHI_diffmin	1.9293	°C
Maximum UHI_diffmin	6.4983	°C

Sky View Photograph

Top-bottom: North, East, South and West.

Average DTR	9.4202	°C
Maximum DTR	15.85	°C
Average NDVI	0.48493	-
Sky View Factor (Holmer et al, 2001)	0.70125	-
built	25	%
impervious	75	%
open	65	%
paved	50	%
vegetated	35	%
water	0	%

location	15	
street	Vergersweg	
latitude	51.974064°	
longitude	5.671387°	
logger	d2243	
local climate zone	6	
Average Summer Temperature	18.664	°C
Minimum Summer Temperature	6.3524	°C
Maximum Summer Temperature	35.986	°C
Average Nighttime Temperature	18.135	°C
Average Daytime Temperature	20.664	°C
Average Summer UHI	1.3366	°C
Average UHI_max	3.0851	°C
Maximum UHI_max	6.3507	°C
Average UHI_diffmin	2.1084	°C
Maximum UHI_diffmin	5.2991	°C

Sky View Photograph

Top-bottom: North, East, South and West.

Average DTR	8.8189	°C
Maximum DTR	15.892	°C
Average NDVI	0.34797	-
Sky View Factor (Holmer et al, 2001)	0.8686	-
built	42.5	%
impervious	92.5	%
open	55	%
paved	50	%
vegetated	10	%
water	0	%

location	16	
street	Haverlanden	
latitude	51.976584°	
longitude	5.666026°	
logger	d2229	
local climate zone	6	
Average Summer Temperature	18.42	°C
Minimum Summer Temperature	6.1382	°C
Maximum Summer Temperature	35.505	°C
Average Nighttime Temperature	18.123	°C
Average Daytime Temperature	20.435	°C
Average Summer UHI	1.0933	°C
Average UHI_max	2.7606	°C
Maximum UHI_max	5.7599	°C
Average UHI_diffmin	1.8422	°C
Maximum UHI_diffmin	5.1415	°C

Sky View Photograph

Top-bottom: North, East, South and West.

Average DTR	8.7776	°C
Maximum DTR	15.542	°C
Average NDVI	0.38054	-
Sky View Factor (Holmer et al, 2001)	0.59717	-
built	25	%
impervious	70	%
open	45	%
paved	45	%
vegetated	30	%
water	0	%

location	17	
street	Hooilandplein	
latitude	51.982718°	
longitude	5.647966°	
logger	d2226	
local climate zone	5-D	
Average Summer Temperature	18.484	°C
Minimum Summer Temperature	6.0867	°C
Maximum Summer Temperature	35.437	°C
Average Nighttime Temperature	18.126	°C
Average Daytime Temperature	20.49	°C
Average Summer UHI	1.1571	°C
Average UHI_max	2.8621	°C
Maximum UHI_max	5.9101	°C
Average UHI_diffmin	1.9458	°C
Maximum UHI_diffmin	4.8051	°C

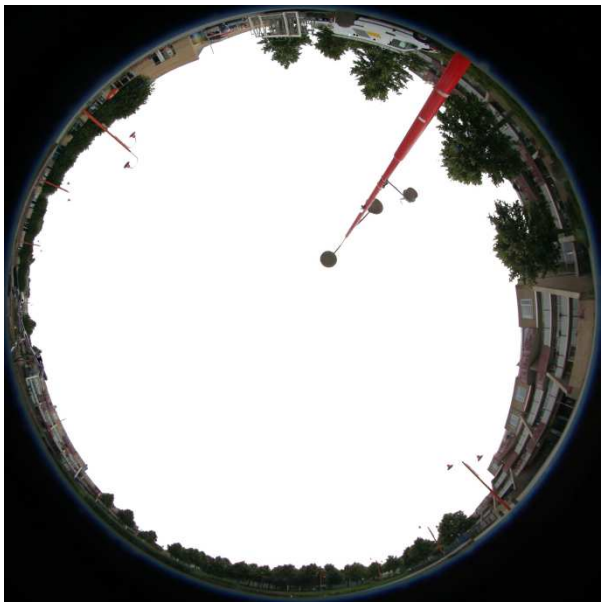

Sky View Photograph

Top-bottom: North, East, South and West.

Average DTR	8.8482	°C
Maximum DTR	16.1	°C
Average NDVI	0.39454	-
Sky View Factor (Holmer et al, 2001)	0.8892	-
built	35	%
impervious	47.5	%
open	42.5	%
paved	12.5	%
vegetated	10	%
water	30	%

location	18	
street	Rietveldlaan	
latitude	51.979093°	
longitude	5.645639°	
logger	d2236	
local climate zone	6	
Average Summer Temperature	18.26	°C
Minimum Summer Temperature	6.1603	°C
Maximum Summer Temperature	33.269	°C
Average Nighttime Temperature	18.122	°C
Average Daytime Temperature	20.311	°C
Average Summer UHI	1.1427	°C
Average UHI_max	2.7689	°C
Maximum UHI_max	5.9103	°C
Average UHI_diffmin	1.8587	°C
Maximum UHI_diffmin	4.6119	°C

Sky View Photograph

Top-bottom: North, East, South and West.

Average DTR	8.9681	°C
Maximum DTR	16.383	°C
Average NDVI	0.44025	-
Sky View Factor (Holmer et al, 2001)	0.552	-
built	45	%
impervious	75	%
open	30	%
paved	30	%
vegetated	25	%
water	0	%

location	19	
street	Markt	
latitude	51.964716°	
longitude	5.663308°	
logger	d2242	
local climate zone	2-5	
Average Summer Temperature	18.783	°C
Minimum Summer Temperature	7.0495	°C
Maximum Summer Temperature	35.624	°C
Average Nighttime Temperature	18.148	°C
Average Daytime Temperature	20.652	°C
Average Summer UHI	1.4528	°C
Average UHI_max	3.4236	°C
Maximum UHI_max	8.2145	°C
Average UHI_diffmin	2.3479	°C
Maximum UHI_diffmin	6.8861	°C

Sky View Photograph

Top-bottom: North, East, South and West.

Average DTR	8.6041	°C
Maximum DTR	15.042	°C
Average NDVI	0.36639	-
Sky View Factor (Holmer et al, 2001)	0.81275	-
built	45	%
impervious	105	%
open	60	%
paved	60	%
vegetated	7.5	%
water	0	%

location	20	
street	Doldersraat	
latitude	51.977252°	
longitude	5.684643°	
logger	d2244	
local climate zone	D	
Average Summer Temperature	18.136	°C
Minimum Summer Temperature	4.4651	°C
Maximum Summer Temperature	35.173	°C
Average Nighttime Temperature	18.099	°C
Average Daytime Temperature	20.623	°C
Average Summer UHI	0.62529	°C
Average UHI_max	1.7719	°C
Maximum UHI_max	5.7051	°C
Average UHI_diffmin	0.79253	°C
Maximum UHI_diffmin	4.4268	°C

Sky View Photograph

Top-bottom: North, East, South and West.

Average DTR	9.8652	°C
Maximum DTR	16.5	°C
Average NDVI	0.53749	-
Sky View Factor (Holmer et al, 2001)	0.8825	-
built	0	%
impervious	7.5	%
open	75	%
paved	7.5	%
vegetated	92.5	%
water	0	%

location	21	
street	Zoomweg	
latitude	51.982679°	
longitude	5.692118°	
logger	d2199	
local climate zone	9-D	
Average Summer Temperature	18.048	°C
Minimum Summer Temperature	5.4513	°C
Maximum Summer Temperature	34.868	°C
Average Nighttime Temperature	18.104	°C
Average Daytime Temperature	20.198	°C
Average Summer UHI	0.72079	°C
Average UHI_max	2.2561	°C
Maximum UHI_max	5.9213	°C
Average UHI_diffmin	1.4658	°C
Maximum UHI_diffmin	4.9063	°C

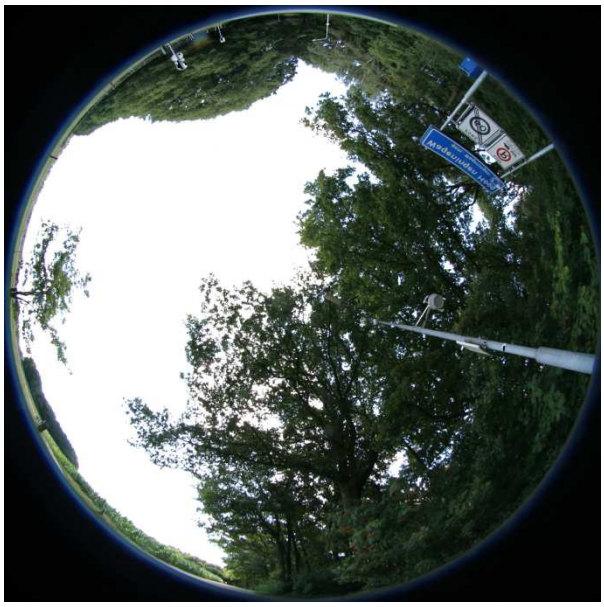

Sky View Photograph

Top-bottom: North, East, South and West.

Average DTR	9.2085	°C
Maximum DTR	16.075	°C
Average NDVI	0.6057	-
Sky View Factor (Holmer et al, 2001)	0.5035	-
built	0	%
impervious	12.5	%
open	45	%
paved	12.5	%
vegetated	80	%
water	0	%

location	22	
street	Droevendaalsesteeg-Campus	
latitude	51.986859°	
longitude	5.665608°	
logger	d2221	
local climate zone	5	
Average Summer Temperature	18.507	°C
Minimum Summer Temperature	5.2735	°C
Maximum Summer Temperature	35.448	°C
Average Nighttime Temperature	18.12	°C
Average Daytime Temperature	20.7	°C
Average Summer UHI	1.1796	°C
Average UHI_max	2.6523	°C
Maximum UHI_max	6.5135	°C
Average UHI_diffmin	1.7232	°C
Maximum UHI_diffmin	5.3185	°C

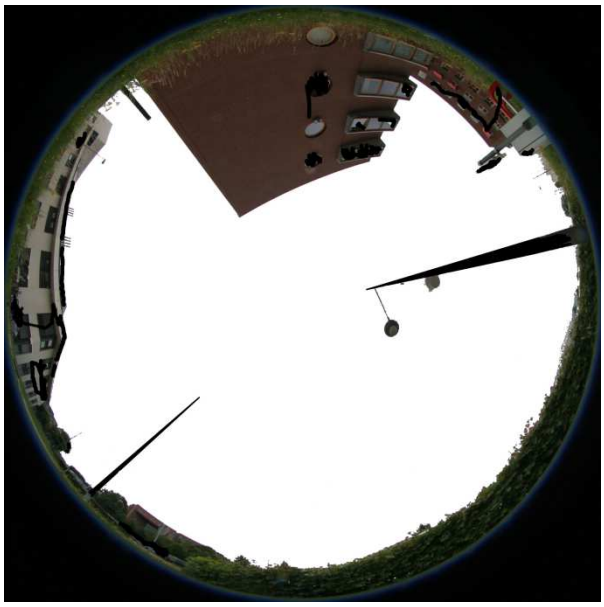

Sky View Photograph

Top-bottom: North, East, South and West.

Average DTR	9.2332	°C
Maximum DTR	15.925	°C
Average NDVI	0.30712	-
Sky View Factor (Holmer et al, 2001)	0.89575	-
built	25	%
impervious	65	%
open	50	%
paved	40	%
vegetated	35	%
water	7.5	%

location	23	
street	Veerweg	
latitude	51.964363°	
longitude	5.682967°	
logger	d2198	
local climate zone	6-D	
Average Summer Temperature	18.108	°C
Minimum Summer Temperature	5.623	°C
Maximum Summer Temperature	34.581	°C
Average Nighttime Temperature	18.102	°C
Average Daytime Temperature	20.441	°C
Average Summer UHI	0.78062	°C
Average UHI_max	2.1505	°C
Maximum UHI_max	6.1463	°C
Average UHI_diffmin	1.3965	°C
Maximum UHI_diffmin	6.0013	°C

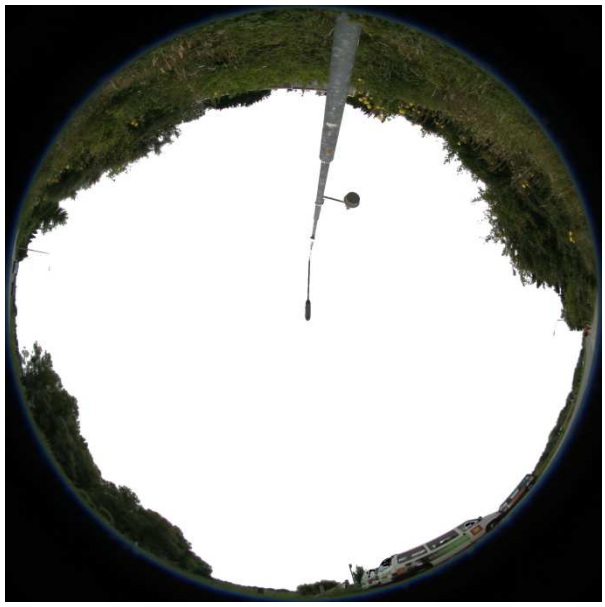

Sky View Photograph

Top-bottom: North, East, South and West.

Average DTR	9.2763	°C
Maximum DTR	16	°C
Average NDVI	0.61206	-
Sky View Factor (Holmer et al, 2001)	0.915	-
built	20	%
impervious	50	%
open	50	%
paved	30	%
vegetated	55	%
water	12.5	%

location	24	
street	Droevendaalsesteeg-Droef	
latitude	51.988691°	
longitude	5.674135°	
logger	d2238	
local climate zone	6	
Average Summer Temperature	17.853	°C
Minimum Summer Temperature	3.9857	°C
Maximum Summer Temperature	34.827	°C
Average Nighttime Temperature	18.072	°C
Average Daytime Temperature	20.425	°C
Average Summer UHI	0.52563	°C
Average UHI_max	1.4958	°C
Maximum UHI_max	3.7391	°C
Average UHI_diffmin	0.61485	°C
Maximum UHI_diffmin	3.7391	°C

Sky View Photograph

Top-bottom: North, East, South and West.

Average DTR	10.264	°C
Maximum DTR	16.608	°C
Average NDVI	0.52703	-
Sky View Factor (Holmer et al, 2001)	0.55725	-
built	40	%
impervious	52.5	%
open	35	%
paved	12.5	%
vegetated	55	%
water	0	%

location	25	
street	Costerweg	
latitude	51.963922°	
longitude	5.658934°	
logger	d2246	
local climate zone	6-8	
Average Summer Temperature	18.411	°C
Minimum Summer Temperature	6.623	°C
Maximum Summer Temperature	34.573	°C
Average Nighttime Temperature	18.122	°C
Average Daytime Temperature	20.44	°C
Average Summer UHI	1.084	°C
Average UHI_max	2.8063	°C
Maximum UHI_max	6.513	°C
Average UHI_diffmin	1.8899	°C
Maximum UHI_diffmin	6.093	°C

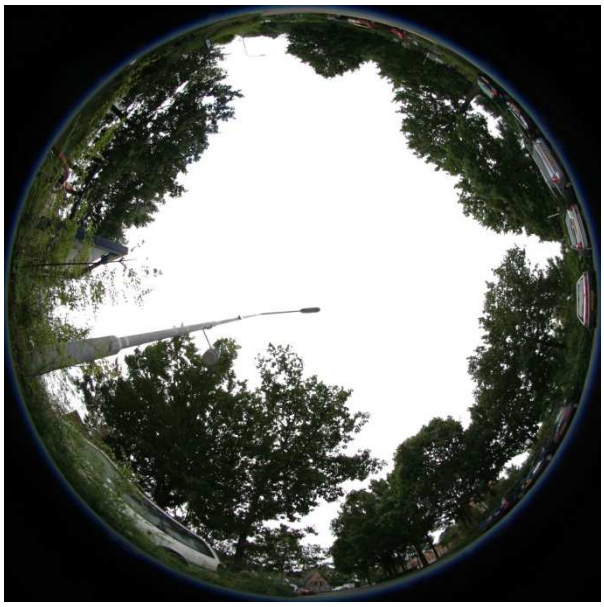

Sky View Photograph

Top-bottom: North, East, South and West.

Average DTR	8.7303	°C
Maximum DTR	15.525	°C
Average NDVI	0.35172	-
Sky View Factor (Holmer et al, 2001)	0.6028	-
built	12.5	%
impervious	57.5	%
open	50	%
paved	45	%
vegetated	20	%
water	0	%

location	26	
street	Groen van Prinsterenstraat	
latitude	51.962544°	
longitude	5.650903°	
logger	d2247	
local climate zone	5	
Average Summer Temperature	18.259	°C
Minimum Summer Temperature	5.9882	°C
Maximum Summer Temperature	34.963	°C
Average Nighttime Temperature	18.119	°C
Average Daytime Temperature	20.251	°C
Average Summer UHI	0.93197	°C
Average UHI_max	2.7152	°C
Maximum UHI_max	5.8149	°C
Average UHI_diffmin	1.6879	°C
Maximum UHI_diffmin	4.4449	°C

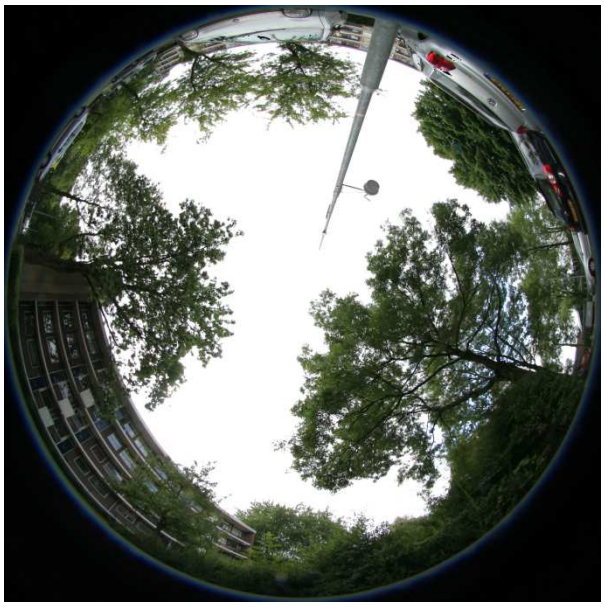

Sky View Photograph

Top-bottom: North, East, South and West.

Average DTR	8.9801	°C
Maximum DTR	15.458	°C
Average NDVI	0.45498	-
Sky View Factor (Holmer et al, 2001)	0.4984	-
built	20	%
impervious	80	%
open	65	%
paved	60	%
vegetated	40	%
water	0	%

location	27	
street	Jachthaven	
latitude	51.955015°	
longitude	5.647390°	
logger	d2231	
local climate zone	9-G	
Average Summer Temperature	18.197	°C
Minimum Summer Temperature	5.9215	°C
Maximum Summer Temperature	34.38	°C
Average Nighttime Temperature	18.114	°C
Average Daytime Temperature	20.28	°C
Average Summer UHI	0.86993	°C
Average UHI_max	2.5238	°C
Maximum UHI_max	5.5999	°C
Average UHI_diffmin	1.6871	°C
Maximum UHI_diffmin	5.5999	°C

Sky View Photograph

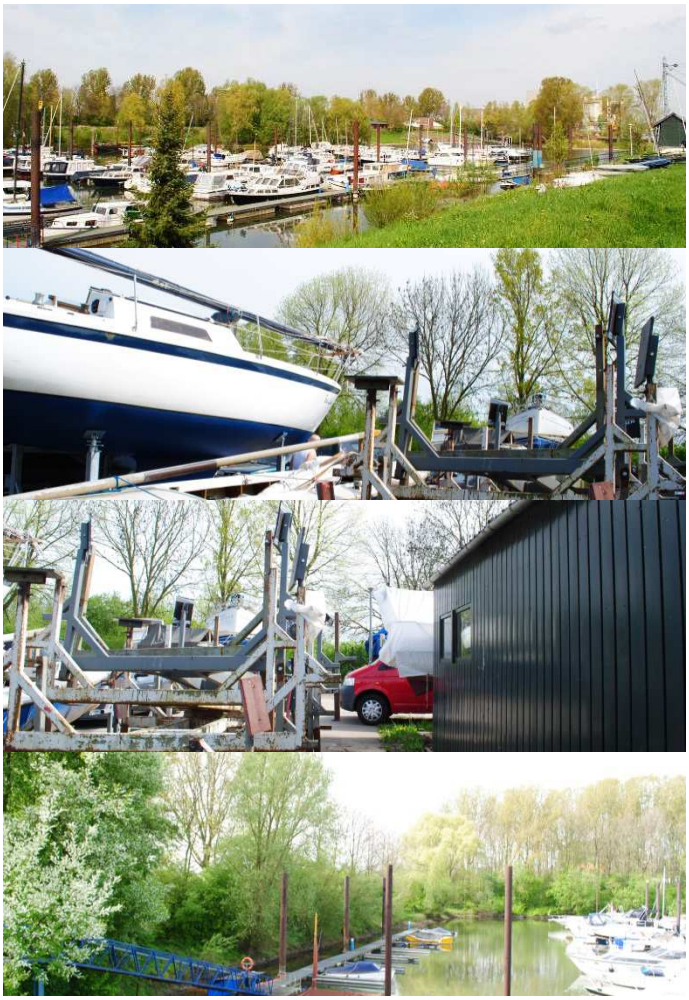

Top-bottom: North, East, South and West.

Average DTR	8.6661	°C
Maximum DTR	15.025	°C
Average NDVI	0.39899	-
Sky View Factor (Holmer et al, 2001)	0.85075	-
built	32.5	%
impervious	67.5	%
open	50	%
paved	35	%
vegetated	40	%
water	25	%

location	28	
street	Thijsselaan	
latitude	51.986981°	
longitude	5.696965°	
logger	d2239	
local climate zone	9	
Average Summer Temperature	17.786	°C
Minimum Summer Temperature	5.7077	°C
Maximum Summer Temperature	34.241	°C
Average Nighttime Temperature	18.104	°C
Average Daytime Temperature	19.74	°C
Average Summer UHI	0.45889	°C
Average UHI_max	2.2594	°C
Maximum UHI_max	5.2443	°C
Average UHI_diffmin	1.5351	°C
Maximum UHI_diffmin	4.736	°C

Sky View Photograph

Top-bottom: North, East, South and West.

Average DTR	8.4756	°C
Maximum DTR	14.717	°C
Average NDVI	0.6112	-
Sky View Factor (Holmer et al, 2001)	0.154	-
built	7.5	%
impervious	20	%
open	12.5	%
paved	12.5	%
vegetated	87.5	%
water	0	%

location	29	
street	Gruttoweide	
latitude	51.977780°	
longitude	5.652634°	
logger	d2197	
local climate zone	6	
Average Summer Temperature	18.267	°C
Minimum Summer Temperature	5.9034	°C
Maximum Summer Temperature	35.153	°C
Average Nighttime Temperature	18.116	°C
Average Daytime Temperature	20.306	°C
Average Summer UHI	0.94012	°C
Average UHI_max	2.5159	°C
Maximum UHI_max	5.4601	°C
Average UHI_diffmin	1.6913	°C
Maximum UHI_diffmin	4.7717	°C

Sky View Photograph

Top-bottom: North, East, South and West.

Average DTR	8.863	°C
Maximum DTR	15.675	°C
Average NDVI	0.4924	-
Sky View Factor (Holmer et al, 2001)	0.5772	-
built	15	%
impervious	57.5	%
open	55	%
paved	42.5	%
vegetated	45	%
water	0	%

location	30	
street	Kees Mulderweg	
latitude	51.973449°	
longitude	5.666387°	
logger	d2232	
local climate zone	5-6	
Average Summer Temperature	18.68	°C
Minimum Summer Temperature	6.1245	°C
Maximum Summer Temperature	36.016	°C
Average Nighttime Temperature	18.132	°C
Average Daytime Temperature	20.752	°C
Average Summer UHI	1.3525	°C
Average UHI_max	2.9981	°C
Maximum UHI_max	6.2328	°C
Average UHI_diffmin	2.0583	°C
Maximum UHI_diffmin	5.1945	°C

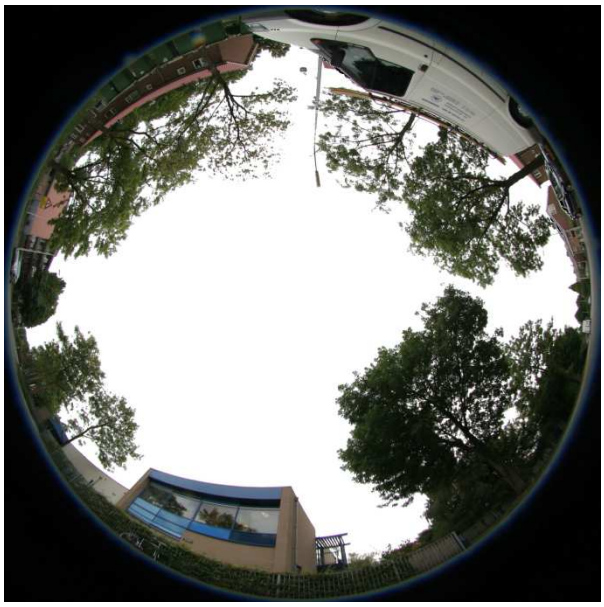

Sky View Photograph

Top-bottom: North, East, South and West.

Average DTR	9.0986	°C
Maximum DTR	15.975	°C
Average NDVI	0.3684	-
Sky View Factor (Holmer et al, 2001)	0.5906	-
built	35	%
impervious	80	%
open	45	%
paved	45	%
vegetated	30	%
water	0	%

location	1	2	3	4	5	6	7	8	9	10
street	Goudenregenstraat	Ceresstraat	Van ‘t Hoffstraat	Ooststeeg	Roghorst	Einthovenstraat	Jagerskamp	Mondriaanlaan	Lombardi	Boeslaan
latitude	51.971997°	51.970020°	51.978244°	51.977161°	51.979936°	51.978622°	51.975493°	51.981079°	51.974688°	51.969768°
longitude	5.677241°	5.671409°	5.672166°	5.658090°	5.666355°	5.677523°	5.679528°	5.653066°	5.657957°	5.686413°
logger	d2225	d2228	d2237	d2245	d2240	d2230	d2234	d2235	d2223	d2194
local climate zone	6	6	5	6	6	6	6	6	9	6
Average Summer Temperature	18.615	18.554	18.511	18.401	18.591	18.647	18.371	18.565	18.411	18.497
Minimum Summer Temperature	6.2058	6.4583	5.9426	5.3799	6.6843	5.6999	5.5166	5.6049	5.1534	6.1415
Maximum Summer Temperature	36.747	35.183	35.218	35.647	35.809	36.125	35.967	35.722	35.378	35.558
Average minimimum temperature	13.868	14.208	13.989	13.747	13.888	13.814	13.626	13.926	13.655	14.001
Max minimum temperature	21.072	22.142	21.168	21.463	20.709	21.225	21.342	21.697	21.728	21.65
Average maximum temperature	23.533	22.737	22.915	22.948	23.219	23.326	22.942	23.062	23.026	23.095
Min maximum temperature	14.606	14.233	14.143	14.263	15.076	14.517	13.967	14.605	15.137	14.225
Average Nighttime Temeprature	18.121	18.134	18.124	18.116	18.127	18.118	18.112	18.121	18.114	18.124
Max nighttime temperature	32.878	32.878	32.878	32.878	32.878	32.878	32.878	32.878	32.878	32.878
Average Daytime Temeprature	20.848	20.492	20.636	20.552	20.814	20.979	20.589	20.753	20.642	20.666
Min daytime temperature	10.056	9.9666	10.068	10.138	10.359	10.392	9.8916	10.263	10.187	10.092
Average UHI	1.2882	1.2273	1.1836	1.0743	1.0783	1.3195	1.0441	1.2379	1.0836	1.17
Minimum UHI	-0.81419	-1.2284	-1.0607	-1.6985	-1.9107	-0.75339	-0.80839	-1.5568	-1.6249	-1.4535
maximum UHI	6.1891	7.7483	5.9343	5.8849	5.6409	6.3416	5.1733	6.4615	6.2184	7.6299
Average UHI_max	2.7756	3.0542	2.7441	2.5599	2.4673	2.7014	2.5792	2.728	2.4668	2.7454
Maximum UHI_max	6.1891	7.7483	5.9343	5.8849	5.6409	6.3416	5.1733	6.4615	6.2184	7.6299
Minimum UHI_max	0.31247	0.35994	0.14927	0.13654	0.10761	0.38161	0.34827	0.17821	0.18507	0.24821
Average UHI_difmin	1.7879	2.0922	1.889	1.6566	1.6409	1.6997	1.5092	1.797	1.5541	1.8811
Maximum UHI_diffmin	4.8175	5.6616	5.4209	4.9565	5.3209	5.2199	4.7616	4.8065	4.9651	6.5382
Minimum UHI_difmin	-0.00586	-0.036727	-0.095727	-0.00846	-0.08906	0.12661	0.0082733	-0.040127	-0.041593	-0.075127
Average DTR	9.6649	8.5291	8.9251	9.2014	9.3308	9.5118	9.3154	9.1366	9.3703	9.0931
Minimum DTR	3.075	2.9333	2.8917	3.075	2.9583	3.0917	2.8667	3.0667	2.75	2.8667
Maximum DTR	16.408	15.925	15.508	16.133	16.075	16.342	15.817	15.983	16.292	16.025
Average NDVI	0.37425	0.32937	0.41315	0.44316	0.47006	0.39706	0.42515	0.46487	0.43668	0.46752
Sky View Factor (Holmer et al, 2001)	0.8045	0.73075	0.7206	0.72733	0.6424	0.747	0.58875	0.6478	0.85275	0.776
SVF (Johnson and Watson,1984)	0.82225	0.742	0.7384	0.73867	0.654	0.7632	0.60075	0.6622	0.86625	0.793
SVF (Matzarakis et al., 2010)	0.59175	0.58875	0.5136	0.57467	0.4686	0.538	0.45225	0.4786	0.68225	0.568
built	35	35	35	20	27.5	27.5	42.5	42.5	25	20
impervious	82.5	82.5	77.5	50	77.5	62.5	75	77.5	45	60
open	55	57.5	45	60	55	35	37.5	35	45	45
paved	47.5	47.5	42.5	30	50	35	32.5	35	20	40
vegetated	25	7.5	25	45	32.5	40	25	35	60	35
water	0	0	0	0	0	0	0	0	0	0

location	11	12	13	14	15	16	17	18	19	20
street	Irenestraat	Thorbeckestraat	Lijnbaanstraat	Hinkeloordseweg	Vergersweg	Haverlanden	Hooilandplein	Rietveldlaan	Markt	Doldersraat
latitude	51.970957°	51.966323°	51.969525°	51.966353°	51.974064°	51.976584°	51.982718°	51.979093°	51.964716°	51.977252°
longitude	5.659366°	5.653608°	5.663064°	5.674717°	5.671387°	5.666026°	5.647966°	5.645639°	5.663308°	5.684643°
logger	d2227	d2195	d2241	d2222	d2243	d2229	d2226	d2236	d2242	d2244
local climate zone	6	5	6	6	6	6	5-D	6	2-5	D
Average Summer Temperature	18.59	18.319	18.704	18.678	18.664	18.42	18.484	18.26	18.783	18.136
Minimum Summer Temperature	6.4632	6.3563	6.4132	6.1617	6.3524	6.1382	6.0867	6.1603	7.0495	4.4651
Maximum Summer Temperature	35.672	34.59	35.813	35.912	35.986	35.505	35.437	33.269	35.624	35.173
Average minimimum temperature	14.135	13.968	14.208	13.996	14.217	13.923	14.025	13.936	14.449	13.065
Max minimum temperature	21.205	20.415	21.155	20.995	21.877	21.43	21.437	21.377	20.599	20.54
Average maximum temperature	22.972	22.467	23.167	23.416	23.036	22.7	22.873	22.904	23.053	22.931
Min maximum temperature	14.588	14.615	14.972	15.287	14.469	14.005	14.495	14.802	11.733	14.848
Average Nighttime Temeprature	18.13	18.126	18.134	18.126	18.135	18.123	18.126	18.122	18.148	18.099
Max nighttime temperature	32.878	32.878	32.878	32.878	32.878	32.878	32.878	32.878	32.878	32.878
Average Daytime Temeprature	20.632	20.197	20.774	20.937	20.664	20.435	20.49	20.311	20.652	20.623
Min daytime temperature	10.08	10.148	10.238	10.17	10.019	10.172	10.228	10.277	10.224	9.9235
Average UHI	1.2629	0.99179	1.377	1.3514	1.3366	1.0933	1.1571	1.1427	1.4528	0.62529
Minimum UHI	-2.4735	-4.047	-2.5235	-2.5833	-0.46426	-1.3818	-0.46993	-6.9081	-2.1955	-1.6765
maximum UHI	6.4699	6.7647	6.9115	8.185	6.3507	5.7599	5.9101	5.9103	8.2145	5.7051
Average UHI_max	2.9477	2.9258	3.0206	2.8242	3.0851	2.7606	2.8621	2.7689	3.4236	1.7719
Maximum UHI_max	6.4699	6.7647	6.9115	8.185	6.3507	5.7599	5.9101	5.9103	8.2145	5.7051
Minimum UHI_max	0.17821	0.19634	0.32821	0.20167	0.40907	0.19487	0.36341	0.28361	0.57281	0.18847
Average UHI_difmin	2.0066	1.9112	2.0886	1.9293	2.1084	1.8422	1.9458	1.8587	2.3479	0.79253
Maximum UHI_diffmin	5.5065	5.3847	5.5915	6.4983	5.2991	5.1415	4.8051	4.6119	6.8861	4.4268
Minimum UHI_difmin	0.0098733	-0.040327	0.11154	-0.13666	0.11741	-0.031793	0.058407	0.03194	0.03114	-0.79319
Average DTR	8.837	8.4993	8.9584	9.4202	8.8189	8.7776	8.8482	8.9681	8.6041	9.8652
Minimum DTR	2.9	2.3083	2.9417	3.1667	2.7917	2.725	2.6083	2.8583	1.1333	2.975
Maximum DTR	15.833	15.525	15.942	15.85	15.892	15.542	16.1	16.383	15.042	16.5
Average NDVI	0.31409	0.40375	0.34134	0.48493	0.34797	0.38054	0.39454	0.44025	0.36639	0.53749
Sky View Factor (Holmer et al, 2001)	0.63775	0.60775	0.8994	0.70125	0.8686	0.59717	0.8892	0.552	0.81275	0.8825
SVF (Johnson and Watson,1984)	0.646	0.621	0.9128	0.72025	0.8818	0.6095	0.9014	0.5652	0.83	0.89475
SVF (Matzarakis et al., 2010)	0.49625	0.44225	0.7242	0.50025	0.6728	0.4162	0.71	0.3832	0.59575	0.707
built	55	25	45	25	42.5	25	35	45	45	0
impervious	75	60	70	75	92.5	70	47.5	75	105	7.5
open	25	40	25	65	55	45	42.5	30	60	75
paved	20	35	25	50	50	45	12.5	30	60	7.5
vegetated	15	50	30	35	10	30	10	25	7.5	92.5
water	0	20	0	0	0	0	30	0	0	0

location	21	22	23	24	25	26	27	28	29	30
street	Zoomweg	Droevendaalsesteeg-Campus	Veerweg	Droevendaalsesteeg-Droef	Costerweg	Groen van Prinsterenstraat	Jachthaven	Thijsselaan	Gruttoweide	Kees Mulderweg
latitude	51.982679°	51.986859°	51.964363°	51.988691°	51.963922°	51.962544°	51.955015°	51.986981°	51.977780°	51.973449°
longitude	5.692118°	5.665608°	5.682967°	5.674135°	5.658934°	5.650903°	5.647390°	5.696965°	5.652634°	5.666387°
logger	d2199	d2221	d2198	d2238	d2246	d2247	d2231	d2239	d2197	d2232
local climate zone	9-D	5	6-D	6	6-8	5	9-G	9	6	5-6
Average Summer Temperature	18.048	18.507	18.108	17.853	18.411	18.259	18.197	17.786	18.267	18.68
Minimum Summer Temperature	5.4513	5.2735	5.623	3.9857	6.623	5.9882	5.9215	5.7077	5.9034	6.1245
Maximum Summer Temperature	34.868	35.448	34.581	34.827	34.573	34.963	34.38	34.241	35.153	36.016
Average minimimum temperature	13.515	13.837	13.518	12.698	13.995	13.752	13.829	13.519	13.761	14.138
Max minimum temperature	20.068	21.79	20.373	19.902	20.415	20.763	19.888	20.166	21.278	21.408
Average maximum temperature	22.723	23.07	22.794	22.962	22.725	22.732	22.495	21.994	22.624	23.236
Min maximum temperature	13.485	14.673	14.898	13.902	14.39	14.43	13.705	13.133	14.628	14.874
Average Nighttime Temeprature	18.104	18.12	18.102	18.072	18.122	18.119	18.114	18.104	18.116	18.132
Max nighttime temperature	32.878	32.878	32.878	32.878	32.878	32.878	32.878	32.878	32.878	32.878
Average Daytime Temeprature	20.198	20.7	20.441	20.425	20.44	20.251	20.28	19.74	20.306	20.752
Min daytime temperature	9.8513	10.257	10.015	10.152	10.048	9.9299	9.7799	9.641	10.12	10.141
Average UHI	0.72079	1.1796	0.78062	0.52563	1.084	0.93197	0.86993	0.45889	0.94012	1.3525
Minimum UHI	-2.007	-0.44153	-3.997	-2.1259	-3.6303	-4.4985	-3.4068	-2.4407	-2.6583	-1.7289
maximum UHI	5.9213	6.5135	6.1463	3.7391	6.513	5.8149	5.5999	5.2443	5.4601	6.2328
Average UHI_max	2.2561	2.6523	2.1505	1.4958	2.8063	2.7152	2.5238	2.2594	2.5159	2.9981
Maximum UHI_max	5.9213	6.5135	6.1463	3.7391	6.513	5.8149	5.5999	5.2443	5.4601	6.2328
Minimum UHI_max	0.30134	0.34681	0.13801	0.15907	0.27467	0.078207	0.01154	-0.063993	0.17674	0.25614
Average UHI_difmin	1.4658	1.7232	1.3965	0.61485	1.8899	1.6879	1.6871	1.5351	1.6913	2.0583
Maximum UHI_diffmin	4.9063	5.3185	6.0013	3.7391	6.093	4.4449	5.5999	4.736	4.7717	5.1945
Minimum UHI_difmin	-0.21533	0.0034733	-0.95366	-0.58259	-0.30366	-0.10013	-0.82179	-0.58066	-0.14493	0.039473
Average DTR	9.2085	9.2332	9.2763	10.264	8.7303	8.9801	8.6661	8.4756	8.863	9.0986
Minimum DTR	2.65	2.825	3.1833	3.275	3.0583	2.7417	3.1083	1.725	2.9	2.875
Maximum DTR	16.075	15.925	16	16.608	15.525	15.458	15.025	14.717	15.675	15.975
Average NDVI	0.6057	0.30712	0.61206	0.52703	0.35172	0.45498	0.39899	0.6112	0.4924	0.3684
Sky View Factor (Holmer et al, 2001)	0.5035	0.89575	0.915	0.55725	0.6028	0.4984	0.85075	0.154	0.5772	0.5906
SVF (Johnson and Watson,1984)	0.507	0.909	0.9255	0.56975	0.616	0.5106	0.86675	0.1585	0.591	0.6044
SVF (Matzarakis et al., 2010)	0.37475	0.7215	0.7555	0.39225	0.4018	0.3092	0.66275	0.05	0.4006	0.3802
built	0	25	20	40	12.5	20	32.5	7.5	15	35
impervious	12.5	65	50	52.5	57.5	80	67.5	20	57.5	80
open	45	50	50	35	50	65	50	12.5	55	45
paved	12.5	40	30	12.5	45	60	35	12.5	42.5	45
vegetated	80	35	55	55	20	40	40	87.5	45	30
water	0	7.5	12.5	0	0	0	25	0	0	0